DMD Fast Forward. Published on April 17, 2008 as DOI: 10.1124/dmd.107.018234
DMD Fast Forward. Published on April 17, 2008 as doi:10.1124/dmd.107.018234
This article has not been copyedited and formatted. The final version may differ from this version.

DMD #18234

BIOTRANSFORMATION OF [^{14}C]DASATINIB: IN VITRO STUDIES IN RAT, MONKEY AND HUMAN AND DISPOSITION AFTER ADMINISTRATION TO RATS AND MONKEYS

Lisa J. Christopher,[1] Donghui Cui[1,2], Wenying Li, Anthony Barros Jr., Vinod K. Arora, Haiying Zhang, Lifei Wang, Donglu Zhang, James A. Manning, Kan He, Anthony M. Fletcher, Marc Ogan, Michael Lago, Samuel J. Bonacorsi, W. Griffith Humphreys, and Ramaswamy A. Iyer*

Departments of Pharmaceutical Candidate Optimization (L.J.C., D.C., W.L., A.B., V.K.A, H.Z., L.W., D.Z., J.A.M., K.H., W.G.H., R.A.I.) Drug Safety Evaluation (A.M.F) and Chemical Synthesis (M.O., M.L., S.J.B.), Bristol-Myers Pharmaceutical Research and Development, Princeton, NJ

Downloaded from dmd.aspetjournals.org at ASPET Journals on April 10, 2024

Copyright 2008 by the American Society for Pharmacology and Experimental Therapeutics.

DMD Fast Forward. Published on April 17, 2008 as DOI: 10.1124/dmd.107.018234
This article has not been copyedited and formatted. The final version may differ from this version.

Running Title: In Vitro-In Vivo Metabolism of Dasatinib

Address: Ramaswamy A. Iyer

Department of Biotransformation

Bristol-Myers Squibb Pharmaceutical Research Institute

P.O. Box 4000, Mail Stop F13-01

Princeton, NJ 08540

Tel: (609) 252-6367

Fax: (609) 252-6802

E-mail: ramaswamy.iyer@bms.com

Text Pages: **45**

Number of Tables: **5**

Number of Figures: **7**

Number of References: **33**

Number of Words in Abstract: **249**

Number of Words in Introduction: **665**

Number of Words in Discussion: **1466**

Abbreviations: ALL, acute lymphoblastic leukemia; BDC, bile-duct cannulated; CML, chronic myelogenous leukemia; CYP, cytochrome P450; FMO, flavin-containing monooxygenase; HPLC, high performance liquid chromatography; LC-MS/MS, liquid chromatography tandem mass spectrometry; LSC, liquid scintillation counting; NAD, nicotinamide adenine dinucleotide; NADP, nicotinamide adenine dinucleotide phosphate; NADPH, nicotinamide adenine dinucleotide phosphate reduced; NMR, nuclear magnetic

Downloaded from dmd.aspetjournals.org at ASPET Journals on April 10, 2024

DMD Fast Forward. Published on April 17, 2008 as DOI: 10.1124/dmd.107.018234
This article has not been copyedited and formatted. The final version may differ from this version.

resonance spectroscopy; PAPS, 3'-phosphoadenosine-5'-phosphosulfate; TRA, Total radioactivity.

Downloaded from dmd.aspetjournals.org at ASPET Journals on April 10, 2024

DMD Fast Forward. Published on April 17, 2008 as DOI: 10.1124/dmd.107.018234
This article has not been copyedited and formatted. The final version may differ from this version.

ABSTRACT

This study describes the *in vitro* metabolism of [^{14}C]dasatinib in liver tissue incubations from rat, monkey and human and the *in vivo* metabolism in rat and monkey. Across species, dasatinib underwent in vitro oxidative metabolism to form five primary oxidative metabolites. In addition to the primary metabolites, secondary metabolites formed from combinations of the oxidative pathways as well as conjugated metabolites of dasatinib and its oxidative metabolites were also observed in hepatocytes incubations. In *in vivo* studies in rats and monkeys, the majority of the radioactive dose was excreted in the bile and feces. In bile-duct cannulated (BDC) monkeys after an IV dose, 13.7% of the radioactive dose was excreted in the feces through direct secretion. Dasatinib comprised of 56% and 26% of the AUC (0-8 h) of total radioactivity (TRA) in plasma, while multiple metabolites accounted for the remaining 44% and 74% of the AUC (0-8 h) of TRA for rats and monkeys, respectively. In rat and monkey bile, dasatinib accounted for <12% of the excreted dose, suggesting that dasatinib was extensively metabolized prior to elimination. The metabolic profiles in bile were similar to the hepatocyte profiles. In both species, a large portion of the radioactivity excreted in bile (≥29% of the dose) was attributed to *N*-oxides and conjugated metabolites. In rat and monkey feces, only the oxidative metabolites and their further oxidation products were identified. The absence of conjugative or *N*-oxide metabolites in the feces suggest hydrolysis or reduction, respectively, in the gastrointestinal tract prior to elimination.

Downloaded from dmd.aspetjournals.org at ASPET Journals on April 10, 2024

DMD Fast Forward. Published on April 17, 2008 as DOI: 10.1124/dmd.107.018234
This article has not been copyedited and formatted. The final version may differ from this version.

INTRODUCTION

SPRYCEL® (dasatinib, BMS-354825, *N*-(2-Chloro-6-methylphenyl)-2-[[6-[4-(2-hydroxyethyl)-1-piperazinyl]-2-methyl-4-pyrimidinyl]amino]-5-thiazolecarboxamide) is a multiple kinase inhibitor that potently inhibits the Bcr-Abl, Src family (SRC, LCK, TES, FYN), cKIT, EPHA2 and PDGFRβ kinases (Lombardo et al., 2004; Das et al., 2006). In *in vitro* cellular assays with transfected murine haematopoietic Ba/F3 cells, dasatinib showed improved potency at inhibiting the kinase activity and cell proliferation of non-mutated BCR-ABL over imatinib (Gleevec®), the current first-line therapy for chronic myelogenous leukemia (CML) (Shah et al., 2004; O'Hare et al., 2005). Dasatinib, at low nanomolar concentrations, was also capable of inhibiting a wide range of imatinib-resistant BCR-ABL isoforms (Shah et al., 2004; Manley et al., 2005; O'Hare et al., 2005). The clinical efficacy of dasatinib has been demonstrated in patients with chronic and accelerated phase CML that is intolerant or resistant to imatinib and in patients with CML in blast crisis (Fricker, 2006; Hampton, 2006). Dasatinib is marketed in the US and EU to treat cancer patients with CML and Philadelphia chromosome-positive acute lymphoblastic leukemia (Ph+ ALL) in patients with Gleevec® (imatinib)-acquired resistance or intolerance. In vitro studies have shown that dasatinib may have clinical efficacy against several types of solid tumors as well (Johnson et al., 2005; Schittenhelm et al., 2006).

Metabolism studies of drug candidates have become an integral part of the drug discovery and development process (Lin et al., 2003; Roberts, 2003). Results from in vitro biotransformation studies can provide early information on metabolic soft spots,

Downloaded from dmd.aspetjournals.org at ASPET Journals on April 10, 2024

DMD Fast Forward. Published on April 17, 2008 as DOI: 10.1124/dmd.107.018234
This article has not been copyedited and formatted. The final version may differ from this version.

potential formation of reactive intermediates, metabolic pathways in different species and possible metabolites formed in humans (Li, 2004). This information may also assist the researcher in developing the appropriate study design for subsequent in vivo studies. Liver microsomes and hepatocytes from animal species and humans have been commonly used in these in vitro metabolism studies (Hewitt et al., 2001; de Graaf et al., 2002). Even though liver microsomes provide useful information on the oxidative metabolic pathways often associated with CYP and FMO enzymes, they don't represent a complete metabolic system. Fresh or cryopreserved hepatocytes from animals and humans are considered complete cell models that contain physiological levels of metabolic enzymes and cofactors (Li et al., 1999). For xenobiotics that are mainly metabolized in the liver, hepatocytes help to predict in vivo metabolic pathways of a drug across species and provide information on the rate of metabolic clearance that can be used for predicting the in vivo pharmacokinetic parameters (Naritomi et al., 2003).

In the current study, we examined the in vitro metabolism of [^{14}C]dasatinib in liver microsomes and hepatocytes from rat, monkey and human and the routes of excretion and extent of metabolism of [^{14}C]dasatinib and its metabolites after administration to rats and monkeys, the species used for long-term toxicology evaluations. In vitro and in vivo metabolic profiles of dasatinib were characterized by radiochromatographic profiling. Dasatinib metabolites were identified by LC/MS/MS and selected metabolites were also isolated and further characterized using NMR. Prior in vitro incubations in hepatocytes and in vivo studies in rats with non-radiolabeled dasatinib had shown that conjugative and oxidative metabolism were involved in the biotransformation of dasatinib and that the compound was extensively metabolized in

Downloaded from dmd.aspetjournals.org at ASPET Journals on April 10, 2024

DMD Fast Forward. Published on April 17, 2008 as DOI: 10.1124/dmd.107.018234
This article has not been copyedited and formatted. The final version may differ from this version.

vivo (Kamath et al., 2008). Therefore, the current studies included administration of [^{14}C]dasatinib to bile-duct cannulated (BDC) animals to understand its overall disposition, particularly for conjugated metabolites excreted in the bile. Conjugative metabolites, for example glucuronides and sulfates, and *N*-oxide metabolites typically undergo further metabolism in the GI by gut flora (deconjugation or reduction) prior to excretion in the feces (Parker et al., 1980; Jaworski et al., 1991; Mitchell et al., 1997; Slatter et al., 2000). Studies were also conducted using both oral- and IV-dosed animals to provide a better understanding of the contributions of direct intestinal secretion and pre-systemic or first-pass metabolism in the excretion of dasatinib. The pharmacokinetics of dasatinib and total radioactivity were examined in plasma from rats and monkeys. Based on the results from in vitro studies and comparison to the in vivo animal data, potential human in vivo biotransformation pathways of dasatinib were proposed.

Downloaded from dmd.aspetjournals.org at ASPET Journals on April 10, 2024

DMD Fast Forward. Published on April 17, 2008 as DOI: 10.1124/dmd.107.018234
This article has not been copyedited and formatted. The final version may differ from this version.

MATERIALS AND METHODS

Chemicals: *N*-(2-chloro-6-methylphenyl)-2-(6-(4-(2-hydroxyethyl)-piperazin-1-yl)-2-methylpyrimidin-4-ylamino)thiazole-5-carboxamide (dasatinib, BMS-354825) with the C-14 label on the 2-carbon of the thiazole ring (Figure 1), and stable-labeled $^{13}C_4$,^{15}N-dasatinib were synthesized by the Radiochemistry Group of the Department of Chemical Synthesis, Bristol-Myers Squibb (New Brunswick, NJ) (Allentoff et al., 2008). Non-radiolabeled dasatinib and reference standards: *N*-(2-chloro-6-methylphenyl)-2-(2-methyl-6-(piperazin-1-yl)pyrimidin-4-ylamino)thiazole-5-carboxamide (*N*-dealkylated amine of dasatinib, M4), 4-(6-(5-(2-chloro-6-methylphenylcarbamoyl)thiazol-2-ylamino)-2-methylpyrimidin-4-yl)-1-(2-hydroxyethyl) piperazine 1-oxide (piperazine *N*-oxide of dasatinib, M5) and 2-(4-(6-(5-(2-chloro-6-methylphenylcarbamoyl)thiazol-2-ylamino)-2-methylpyrimidin-4-yl)piperazin-1-yl)acetic acid (carboxylic acid metabolite of dasatinib, M6) were synthesized chemically at Bristol-Myers Squibb Research and Development (Princeton, NJ) (Figure 1). [^{14}C]Dasatinib with a radiochemical purity of 97.9% and a specific activity of 30.4 μCi/mg, was used for *in vitro* studies. [^{14}C]Dasatinib with a radiochemical purity of 97.9% and a specific activity of 27.5 μCi/mg was used in the study with bile duct-cannulated rats; and [^{14}C]dasatinib with a radiochemical purity of 99.5% and a specific activity of 17.0 μCi/mg was used in the studies with intact rats, intact monkeys, and bile duct-cannulated monkeys.

All reagents were purchased from Sigma-Aldrich Chemical Co. (St. Louis, MO), except where indicated. Solvents used for HPLC analysis were of HPLC grade. IN-Flow 2:1™ (INUS Systems, Tampa, FL) was used as the scintillation cocktail for on-line radioactivity detection. Ecolite™ scintillation cocktail was obtained from MP

Downloaded from dmd.aspetjournals.org at ASPET Journals on April 10, 2024

DMD Fast Forward. Published on April 17, 2008 as DOI: 10.1124/dmd.107.018234
This article has not been copyedited and formatted. The final version may differ from this version.

Biomedicals (Irvine, CA) and Emulsifier-Safe and Permofluor E+ scintillation fluid, and Soluene®-350 were obtained from PerkinElmer Life Sciences, Inc. (Boston, MA). Gas cylinders containing 95% O_2:5% CO_2 were purchased from Airgas Inc. (Piscataway, NJ). Rat hepatocytes were prepared at Bristol-Myers Squibb according to a standard literature procedure (Pang et al., 1995). Cryopreserved cynomolgus monkey (male, pooled, n=6) and human hepatocytes (from 3 individual donors) were purchased from In Vitro Technologies (Baltimore, MD). Microsomes from male Sprague-Dawley rats (20 mg/mL) and male cynomolgus monkeys (20 mg/mL) were obtained from Xenotech LLC, (Kansas City, KS). Male human liver microsomes (20 mg/mL) and male human liver cytosol (10 mg/mL) were from BD Biosciences (Woburn, MA).

Hepatocyte Incubations: Modified Krebs-Henseleit buffer was prepared as follows: Krebs-Henseleit buffer powder (9.6 g), sodium bicarbonate (2.1 g), glucose (1.6 g) and calcium chloride dihydrate (0.37 g) were dissolved in ultrapure water to a final volume of 1 L. The buffer was bubbled with 95% O_2:5% CO_2 on ice for approximately 1 h (final pH = 7.4). Human and monkey cryopreserved hepatocytes were thawed and prepared in Krebs-Henseleit buffer. The viability of the hepatocytes from rat, monkey, and human was evaluated using a Trypan Blue exclusion assay and a hemocytometer. The initial viability of the hepatocytes ranged from 77% to 90%. The cell suspensions were diluted accordingly with modified Krebs-Henseleit buffer to give a final concentration of 2 million cells/mL.

Incubations were conducted at 37 ºC for 3 h in a NAPCO CO_2 6000 incubator (VWR Scientific Products) under a 95% air and 5% CO_2 atmosphere. The incubation

Downloaded from dmd.aspetjournals.org at ASPET Journals on April 10, 2024

DMD Fast Forward. Published on April 17, 2008 as DOI: 10.1124/dmd.107.018234
This article has not been copyedited and formatted. The final version may differ from this version.

samples were shaken at 90 rpm with an orbital shaker. Each incubation contained 20 μM [^{14}C]dasatinib and ~2 million cells/mL. A control incubation, in the absence of hepatocytes, was also performed. The incubations were stopped by adding one volume of ice-cold acetonitrile. The resulting mixture was vortex mixed, centrifuged for 5 min at 13,000 rpm and the supernatant was dried under nitrogen (TurboVap, Zymark Corp., Hopkinton, MA). The residues were reconstituted into acetonitrile/water (30:70 v/v) and analyzed by HPLC-MS and on-line radiochemical detection.

Liver Microsome and Cytosol Incubations: Each 0.5 mL incubation contained 0.1 M potassium phosphate buffer (pH 7.4), 2.5 mM $MgCl_2$, 2 mg/mL microsomal or cytosolic proteins, and 2.0 mM of cofactor (NADPH, NAD^+, $NADP^+$ or 3'-phosphoadenosine-5'-phosphosulfate (PAPS)). The concentration of substrate ([^{14}C]dasatinib or non-labeled dasatinib) was 20 μM in all the incubations. Stock solutions of 4-methylpyrazole and disulfiram were prepared in acetonitrile and the final concentration of each inhibitor was 100 μM. The mixtures were preincubated in a shaking water bath at 37^{o}C for 2 min and cofactors were added to start the reactions. Incubations were continued for 15 or 60 min for microsomes and 60 min for cytosol incubations. Control incubations in the absence of proteins or cofactors were performed. The reactions were stopped with the addition of 1 mL of ice-cold acetonitrile. The mixtures were vortex mixed, centrifuged, and the supernatants were transferred into new test tubes. The supernatants were then dried under nitrogen and the residues were reconstituted in acetonitrile/water (30:70 v/v). The samples were analyzed by HPLC-MS and on-line radiochemical detection.

Downloaded from dmd.aspetjournals.org at ASPET Journals on April 10, 2024

DMD Fast Forward. Published on April 17, 2008 as DOI: 10.1124/dmd.107.018234
This article has not been copyedited and formatted. The final version may differ from this version.

Dosing of Animals and Collection of Samples: All animal studies were conducted after approval of protocols by the Institutional Animal Care and Use Committee (IACUC) in approved facilities.

Intact rat study: The mass-balance and pharmacokinetics of radioactivity and metabolism of dasatinib were investigated in intact male Sprague-Dawley rats (Harlan) after administration of [^{14}C]dasatinib. A total of 18 rats, weighing approximately 340-380 g, were divided into three groups. Each rat received a single dose of [^{14}C]dasatinib (15 mg (80 μCi)/kg, 5 mL/kg) orally by gavage. The dosing vehicle was 80 mM sodium citrate buffer (pH 3.1). The rats were fasted overnight prior to dosing and food was returned at 4 h post-dose. One group of rats (*n = 3*) was individually housed in metabolism cages for the separate collection of urine and feces. The excreta were collected into containers surrounded by dry ice for the 21 h interval prior to dosing and at various time intervals through 168 h after dose administration. Cage rinses were performed after each collection interval and a cage wash was performed at the end of the study period. Serial blood samples for pharmacokinetic analysis of radioactivity were collected from a second group of rats (*n = 3*). Blood samples (approximately 0.3 mL) were drawn before dosing and at 0.25, 0.5, 1, 2, 3, 4, 6, 8, 12, 24, 48, 72, 96, 120, 144, and 168 h post-dose from tail vein, jugular vein or puncture of the retro-orbital plexus following CO_2 anesthesia. Terminal blood samples (maximum volume) for biotransformation profiling were collected via cardiac puncture after CO_2 anesthesia from the third group of rats (*n = 3* rats per time point) at 1, 4, 8 and 24 h post-dose.

Bile Duct-Cannulated Rat Study: The excretion of radioactivity into bile and urine, and metabolism of dasatinib were investigated in bile duct-cannulated male Sprague-Dawley

Downloaded from dmd.aspetjournals.org at ASPET Journals on April 10, 2024

DMD Fast Forward. Published on April 17, 2008 as DOI: 10.1124/dmd.107.018234
This article has not been copyedited and formatted. The final version may differ from this version.

rats (Harlan), after oral or intravenous (IV) administration of [^{14}C]dasatinib. In addition, biotransformation profiles of dasatinib in plasma were obtained after oral or intravenous (IV) administration of [^{14}C]dasatinib to intact rats. A total of 16 rats (4 bile duct-cannulated and 12 intact, weighing between 220-325 g), divided into 4 groups were assigned to the study. Two groups (*n = 2* bile duct cannulated and *n = 6* intact) received a single dose of [^{14}C]dasatinib (10 mg (60 μCi)/kg, 5 mL/kg) administered orally by gavage. The other two groups (*n = 2* bile duct cannulated and *n = 6* intact) received a single dose of [^{14}C]dasatinib (10 mg (60 μCi)/kg, 5 mL/kg) administered as a 10 min IV infusion via a catheter placed in the jugular vein. The dosing vehicle was sodium acetate buffer (pH 4.0) for both routes of administration. All rats were fasted overnight and for the duration of the study. The two groups of BDC animals were individually housed in metabolism cages. During the period of sample collection, bile salts were replenished by infusing control bile, collected in the days prior to dose administration, at a rate of 1 mL/h. Urine and bile were collected into containers surrounded by ice prior to dosing and at 0-12 h after dose administration. At the end of the study period, the gastrointestinal tract and its contents were ligated and excised from the BDC rats that had received an oral dose of dasatinib. Terminal blood samples (maximum volume) for biotransformation profiling were collected via cardiac puncture after CO_2 anesthesia from intact rats (*n = 2* rats per route of administration per time point) at 1, 4, and 8 h post-dose.

Intact monkey study: The mass-balance and pharmacokinetics of radioactivity and metabolism of dasatinib were investigated in intact male cynomolgus monkeys (Charles River Laboratories), after administration of [^{14}C]dasatinib. The monkeys (*n = 3*), weighing between 4-5 kg, each received a single dose of [^{14}C]dasatinib [10 mg (30

Downloaded from dmd.aspetjournals.org at ASPET Journals on April 10, 2024

DMD Fast Forward. Published on April 17, 2008 as DOI: 10.1124/dmd.107.018234
This article has not been copyedited and formatted. The final version may differ from this version.

μCi)/kg, 2.5 mL/kg] orally by gavage. The dosing vehicle was 80 mM sodium citrate buffer (pH 3.1). The monkeys were fasted overnight prior to dosing and food was returned at 4 h post-dose. The animals were individually housed in metabolism cages. Urine was collected into containers surrounded by dry ice and feces were collected at ambient temperature prior to dosing and at various time intervals through 168 h after dose administration. Cage rinses were performed after each collection interval and a cage wash was performed at the end of the study period. Serial blood samples for pharmacokinetic analysis of radioactivity (approximately 1 mL) were drawn before dosing and at 0.25, 0.5, 1, 2, 3, 4, 6, 8, 12, 24, 48, 72, 96, 120, 144, and 168 h post-dose from a venous catheter and vascular access port. Blood samples (approximately 5 mL) for biotransformation profiling were collected in conjunction with the pharmacokinetic blood samples at 1, 4, 8 and 24 h post-dose.

Bile Duct-Cannulated Monkey Study: The excretion of radioactivity into bile, urine and feces, pharmacokinetics of radioactivity and metabolism of dasatinib were investigated in male bile duct-cannulated cynomolgus monkeys (Charles River Laboratories), after administration of [^{14}C]dasatinib. The monkeys (*n = 3*), weighing between 4-6.5 kg, each received a single dose of [^{14}C]dasatinib (2 mg (30 μCi)/kg, 1 mL/kg) as a 10 min IV infusion via a temporary percutaneous catheter placed in a saphenous or cephalic vein. The dosing vehicle was 80 mM sodium citrate buffer (pH 3.1). The monkeys were fasted overnight prior to dosing and food was returned at 4 h post-dose. The animals were individually housed in metabolism cages. Urine and bile were collected into containers surrounded by dry ice and feces were collected at ambient temperature prior to dosing and at various time intervals through 72 h after dose administration. Blood samples

Downloaded from dmd.aspetjournals.org at ASPET Journals on April 10, 2024

DMD Fast Forward. Published on April 17, 2008 as DOI: 10.1124/dmd.107.018234
This article has not been copyedited and formatted. The final version may differ from this version.

(approximately 5 mL) for analysis of radioactivity and biotransformation profiling were collected via an indwelling venous catheter and vascular access port at 1, 4, 8, 24 and 72 h post-dose. During the course of the study, bile salts were replaced via the distal flushing catheter. The volume of bile salts administered was approximately 23 mL/kg/day.

Toxicokinetic studies in rats and monkeys: Plasma concentrations of dasatinib were obtained from separate toxicokinetic (TK) studies in which rats and monkeys were administered a 10 mg/kg oral dose of non-radiolabeled dasatinib. Blood was collected from rats ($n = 3$ per time point) at 1, 2, 4, 6, and 8 h post dose, and monkeys ($n = 3$) at 1, 2, 4, 8, 12, and 24 h post-dose, and plasma was prepared. Plasma concentrations of dasatinib were determined with validated liquid chromatography-tandem mass spectrometry methods (LC/MS/MS). Details of the TK study and LC/MS/MS methods will be the subject of a separate manuscript. The plasma concentrations of dasatinib obtained from these studies are presented here to illustrate the contribution of dasatinib to the overall profile of drug-related components.

For all in vivo studies, blood samples were collected into Vacutainer® tubes containing ethylenediaminetetraacetic acid (EDTA) as an anticoagulant. After collection, the tubes were immediately placed on ice until processing. Within 1 h of collection, plasma was prepared from blood by centrifugation. Water was added to each fecal sample to form a 20% (w/w feces/water) fecal homogenate. Water was added to each GI tract sample from orally-dosed BDC rats to form a 25% (w/w GI tract/water) homogenate. The fecal and GI tract samples were homogenized using a probe-type homogenizer (Kinematica Polytron Model No. PT 45/80 or PT 3100, Brinkman Instruments, Fullerton, CA).

Downloaded from dmd.aspetjournals.org at ASPET Journals on April 10, 2024

DMD Fast Forward. Published on April 17, 2008 as DOI: 10.1124/dmd.107.018234
This article has not been copyedited and formatted. The final version may differ from this version.

Analysis of Radioactivity: Aliquots of plasma (50-100 µL), bile and urine (50-300 µL) and cage wash/rinse samples (300 µL volumes) were added to 5-15 mL of scintillation cocktail (Emulsifier-Safe, or Ecolite™) and analyzed directly by liquid scintillation counting. Aliquots of GI or feces homogenate from the BDC rat study (approximately 0.2 g each) were incubated overnight at 60°C with Soluene-350 to solubilize the samples. Upon cooling, 0.2 mL of 30% hydrogen peroxide was added to each sample to de-color. Known amounts of samples were mixed with scintillation cocktail (Emulsifier-Safe, or Ecolite™) and counted on a LS 6000 or LS 6500 liquid scintillation counter (Beckman Instruments, Inc., Fullerton, CA), or on a Packard Tricarb 3200CA liquid scintillation counter (PerkinElmer Life Sciences). In other studies, aliquots of fecal homogenates 0.2-0.5 g were air dried before combustion using a Model 307 or Model 387 Sample Oxidizer (PerkinElmer Life Sciences). The liberated $^{14}CO_2$ was trapped into Carbo-Sorb E (PerkinElmer Life Sciences), mixed with Permafluor E+ scintillation fluid and analyzed by liquid scintillation counting. The efficiency of the sample oxidizer was determined prior to combusting experimental samples. Three levels of radioactivity corresponding to low, medium, and high [^{14}C]-standards were placed into cones and pads, and combusted. The combusted standards were analyzed by liquid scintillation counting along with scintillation fluid that was spiked with equivalent levels of the [^{14}C]-standards. The average disintegrations per minute (dpm) in combusted samples was compared with the spiked samples to determine the combustion efficiency. Combustion efficiency for fecal samples was considered acceptable if the recovery of radioactivity was ≥ 90%. The radioactivity in plasma, urine, bile and feces were reported as ng-eq dasatinib/g or as a percentage of the administered dose.

Downloaded from dmd.aspetjournals.org at ASPET Journals on April 10, 2024

DMD Fast Forward. Published on April 17, 2008 as DOI: 10.1124/dmd.107.018234
This article has not been copyedited and formatted. The final version may differ from this version.

Pharmacokinetic Analysis: Determination of radioequivalents, and statistical analysis of radioactivity measurements were performed using Microsoft Excel (2002, Microsoft Corporation, Redmond, Washington) and Debra® ADME software (Version 5, Lablogic Systems Ltd., Sheffield, England). The AUC (0-8 h) values for TRA and dasatinib were determined by a non-compartmental analysis of plasma concentration versus time data (KINETICA™ software, Version 4.2, InnaPhase Corporation, Philadelphia, PA). Plasma concentrations of TRA were obtained from studies where [^{14}C]dasatinib was administered to rats and monkeys. Dasatinib plasma concentrations were obtained from separate TK studies where non-radiolabeled dasatinib was administered. The concentrations of TRA and dasatinib at 1, 2, 4, 6, and 8 h post-dose for rats, and 1, 2, 4, and 8 h post-dose for monkeys were used in the AUC (0-8 h) calculations.

Preparation of Samples for Radiochromatographic and Mass-Spectral Analysis of Metabolites: Plasma samples (1-3 mL), pooled by timepoint, were extracted with 2 volumes of acetonitrile/methanol (50:50 v/v). Fecal homogenates (approximately 0.2 g, 0.2 mL), pooled over the 0-168 h collection interval, were extracted with 3 volumes of acetonitrile/methanol (50:50 v/v). Monkey urine, pooled over the 0-168 h collection interval, was extracted with 2 volumes of acetonitrile/acetone (50:50 v/v). After centrifugation at 2,000 x g for 10 min (4°C), the supernatants from the plasma, fecal, or urine extractions were evaporated to dryness under a stream of nitrogen gas, and the residues were reconstituted in acetonitrile/water (35:65 v/v for feces or 30:70 v/v for plasma and urine).

Rat urine samples, pooled over the 0-168 h interval, were centrifuged at 16,000 x g for 10 min (4°C) and the supernatants were analyzed directly.

Downloaded from dmd.aspetjournals.org at ASPET Journals on April 10, 2024

DMD Fast Forward. Published on April 17, 2008 as DOI: 10.1124/dmd.107.018234
This article has not been copyedited and formatted. The final version may differ from this version.

Bile samples from BDC rats (0.2 mL), pooled over the 0-12 h interval, were diluted 6-fold with water and loaded onto a Waters Oasis™ HLB solid-phase extraction cartridges (SPE, 1cc, Waters Corporation, Milford, MA). The extracted components were eluted with 2 mL of 0.1% formic acid in methanol. The column eluate was evaporated to dryness under nitrogen gas and the dried residues were reconstituted in acetonitrile/water (50:50 v/v).

Bile from BDC monkeys, pooled over the 0-72 h interval, was diluted 15-fold with acetonitrile/water (20:80 v/v) containing 0.1% formic acid. The diluted sample was centrifuged at 16,000 x g for 5 min and the supernatant was analyzed.

Radiochromatographic Analysis of Metabolites: Radiochromatographic analysis of samples from *in vitro* studies was performed on a Waters Alliance™ HPLC system equipped with Waters model 2695 binary pumps and a photodiode array detector (Waters model 2996, Waters, Milford, MA). A Phenomenex Synergi Polar-RP® column (4.6 x 250 mm, 4 micron, Phenomenex, Torrance, CA) maintained at 30°C was used for metabolite separation. All HPLC analyses were performed at a flow rate of 1 mL/min. Two HPLC mobile phase and gradient systems were used. The first system consisted of mobile phases (A) water with 0.1% formic acid and (B) acetonitrile with 0.1% formic acid. The gradient program was as follows: hold isocratic at 20% B (0-1 min); linear gradient from 20-35% B (1-41 min); linear gradient from 35-90% B (41-42 min); hold isocratic at 90% B (42-44 min). The column was re-equilibrated at 20% B for 6 min before the next injection. The second HPLC system was used to separate certain co-eluting metabolites that were not resolved on the first system. The mobile phase consisted of (A) water with 0.1% triflouroacetic acid (TFA) and (B) acetonitrile with 0.1% TFA.

Downloaded from dmd.aspetjournals.org at ASPET Journals on April 10, 2024

DMD Fast Forward. Published on April 17, 2008 as DOI: 10.1124/dmd.107.018234
This article has not been copyedited and formatted. The final version may differ from this version.

The gradient was as follows: hold isocratic at 20% B (0-1 min); linear gradient from 20-35% B (1-51 min); linear gradient from 35-90% B (51-52 min); hold isocratic at 90% B (52-54 min). The column was equilibrated at 20% B for 6 min prior to the next injection. Only radioprofiles from in vitro samples obtained with the first HPLC system are presented here.

Radiochromatographic analysis of rat bile extracts was performed on a Shimadzu HPLC system (Shimadzu Corporation, Columbia, MD), equipped with two 10AD VP® pumps, a SIL-10AD autoinjector, a model SCL-10A system controller and a SPD-M10A photodiode array detector. The column temperature was maintained at 35°C with an Eppendorf TC-45 controller and CH-30 column heater. Separation of metabolites was achieved on a YMC™ ODS-AQ column (3.0 x 150 mm, 3-µm particle size, Waters Corporation). The mobile phase contained (A) 0.1% TFA in water and (B) 0.1% TFA in acetonitrile; the flow rate was 0.4 mL/min. The gradient program used for elution of the metabolites was as follows: hold isocratic at 5% B, (0-1 min); linear gradient from 5-15% B (1-5 min); linear gradient from 15-32% B (5-52 min); linear gradient from 32-95% B (52-55 min); hold isocratic at 95% B (55-60 min); re-equilibrate at 5% B for 9 min.

Radiochromatographic analysis of plasma, urine and fecal samples from rat and monkey, and monkey bile samples was performed on an Agilent 1100™ HPLC system equipped with binary pumps, autoinjector, column heater and vacuum degasser. Metabolites were separated on a Phenomonex (4.6 x 250 mm, 4-µm particle size) Synergi Polar-RP® column (Phenomonex Torrance, CA). The column temperature was maintained at 35°C. The mobile phase consisted of (A) 0.1% formic acid in water and (B) 0.1% formic acid in acetonitrile; the flow rate was 1.0 mL/min. The gradient program

Downloaded from dmd.aspetjournals.org at ASPET Journals on April 10, 2024

DMD Fast Forward. Published on April 17, 2008 as DOI: 10.1124/dmd.107.018234
This article has not been copyedited and formatted. The final version may differ from this version.

used for elution of the metabolites was as follows: hold isocratic at 15% B (0-3 min); linear gradient from 15-32% B (3-53 min); hold isocratic at 32% B (53-53.5 min); linear gradient from 32-90% B (53.5-60 min); hold isocratic at 90% B (60-63 min); re-equilibrate at 15% B for 6 min.

The distribution of ^{14}C-labeled metabolites of dasatinib in microsomal and hepatocyte incubations was monitored using a flow-through radiochemical detector for HPLC (β-RAM Model 3, IN/US, Tampa, FL). The HPLC effluent was split between the radiochemical detector and mass spectrometer at a ratio of 9 to 1. The β-RAM was operated in the homogeneous liquid scintillation counting mode and a 500-μL flow cell and a flow rate of 2 mL/min of scintillation cocktail were used for all the analyses. The percentage of each chromatographic peak was obtained through integration of the peak, and metabolites were quantified and expressed as percentage of the total radioactivity in the sample. Recovery of radioactivity from the HPLC column was evaluated by comparing the amount of radioactivity injected (determined using LSC) and the amount of total radioactivity detected by the β-RAM.

For samples from in vivo studies, the column eluate was collected in 96-well Packard Lumaplates® (PerkinElmer Life Sciences) over 0.25 min intervals with a Gilson Model FC 204 Fraction Collector (Gilson, Mideleton, WI). The plates were dried on a Savant Speed-Vac (Savant Instruments Inc., Holbrook, NY) and were counted for 10 min per well with a Top Count microplate scintillation analyzer (PerkinElmer Life Sciences) to quantify radioactivity. Radiochromatographic metabolite profiles were prepared by plotting the net CPM values obtained from the Top Count versus time after injection using Microsoft Excel (Microsoft Corporation). The metabolites were quantified based

Downloaded from dmd.aspetjournals.org at ASPET Journals on April 10, 2024

DMD Fast Forward. Published on April 17, 2008 as DOI: 10.1124/dmd.107.018234
This article has not been copyedited and formatted. The final version may differ from this version.

on the percentage of total radioactivity in each peak relative to the entire radiochromatogram (Zhu et al., 2005).

Mass Spectrometry: Mass spectral analysis was performed on a Finnigan LCQ or LCQ Deca ion trap mass spectrometer equipped with an ESI probe (Thermo Fisher Scientific, Waltham, MA). Analyses were performed in the positive ion mode. Samples were introduced into the mass-spectrometer with the same HPLC conditions used for radioprofiling. For HPLC conditions where a flow rate of 0.4 mL/min was employed, the entire column eluate was introduced into the mass spectrometer. For conditions where a flow rate of 1 mL/min was used, the flow was split such that approximately 0.15 mL/min was directed into the mass-spectrometer. High purity nitrogen was used as the sheath and the auxiliary gas with levels at 60 and 10 (relative flow rate), respectively. The capillary temperature was 275^{o}C (LCQ) and 320°C (LCQ Deca). Other parameters were adjusted as needed to achieve maximum sensitivity.

Accurate mass data were acquired on a Finnigan LTQ-FT instrument equipped with a NanoMate nanospray apparatus (Thermo Fisher Scientific, Waltham, MA). Analysis was performed in the +ESI mode. The FT mass resolution setting was 12500. The mass isolation window for the MS^n scans was 6 Da. The activation time was 100 ms. The collision energy varied from 15% to 45% for optimal spectral quality.

Isolation of Metabolites M20 and M24 for NMR Analysis: A large-scale incubation (100-mL) of dasatinib, at a concentration of 0.1 mM, with human liver microsomes was conducted in order to generate metabolites M20 and M24. Incubations were conducted in 0.1 M potassium phosphate buffer (pH 7.4) at 37^{o}C for 90 min. The incubation mixture contained 2 mg/mL microsomal protein, 5 mM NADPH, 2.5 mM $MgCl_2$ and 5% (v/v)

Downloaded from dmd.aspetjournals.org at ASPET Journals on April 10, 2024

DMD Fast Forward. Published on April 17, 2008 as DOI: 10.1124/dmd.107.018234
This article has not been copyedited and formatted. The final version may differ from this version.

methanol. The reaction was stopped by adding an equal volume of cold acetonitrile. After removal of the protein pellet by centrifugation, solvent was evaporated under vacuum to generate a white residue, which was then dissolved in methanol.

Metabolites M20 and M24 were isolated using a Dionex semi-prep HPLC system (Sunnyvale, CA) equipped with a YMC ODS-AQ 20 x150 mm column (Waters, Milford, MA) and a mobile phase consisting of (A) 0.1% formic acid in water, and (B) 0.1% formic acid in acetonitrile. The flow rate was 10 mL/min for the entire run. The gradient was as follows: initial conditions 5% B; linear gradient from 5-15% B (0-5 min); hold isocratic at 15% B (5-31 min); followed by a column wash with 80% B. The column was re-equilibrated at 5% for 10 min. Fractions containing M20 and M24 were pooled separately and lyophilized. Approximately 1.5 mg of M20 and 0.3 mg of M24 were isolated as their formic acid salts.

NMR Analysis: The metabolite samples and dasatinib were dissolved in DMSO-d_6 and analyzed by a Bruker Avance 700 MHz NMR spectrometer equipped with a 5 mm cryo triple resonance probe (Bruker, Billerica, MA) at room temperature. All ^{1}H chemical shifts are reported on the δ scale (parts per million) downfield from tetramethylsilane using the DMSO-d_6 lock signal as reference at δ2.50 ppm. ^{13}C chemical shift data were deduced from HMBC and HMQC spectra, and were referenced to DMSO-d_6 at δ39.5 ppm. The peak assignment was based on: ^{1}H, ^{1}H-^{1}H-gCOSY, ^{1}H-^{13}C-HMBC, and ^{1}H-^{13}C-HMQC analysis. ACD/NMR prediction software was obtained from Advanced Chemistry Development Inc. (Toronto, ON, Canada).

Downloaded from dmd.aspetjournals.org at ASPET Journals on April 10, 2024

DMD Fast Forward. Published on April 17, 2008 as DOI: 10.1124/dmd.107.018234
This article has not been copyedited and formatted. The final version may differ from this version.

RESULTS

Biotransformation Profiles in Microsomes and Hepatocytes: Metabolites of dasatinib were numbered based on their chronologies of identification and did not follow HPLC elution order. Representative radiochromatographic profiles from extracts of rat, monkey, and human liver microsome and hepatocyte incubations are shown in Figures 2A and 2B, respectively. The extent of metabolism, defined as the percentage of dasatinib (20 μM) converted to its metabolites over a period of 15 min, was 46, 73, and 65% for rat, monkey, and human liver microsomes, respectively. In hepatocytes, after a 3 h incubation period, the extent of dasatinib (20 μM) metabolism was 11, 39, and 22% for rat, monkey, and human, respectively.

The structures of metabolites identified in microsomes and hepatocytes from the three species are shown along with in vivo metabolites found in rat and monkey in Figure 1. Metabolites M20 and M24 were the most abundant metabolites in monkey and human liver microsomes, accounting for 30 and 39% of total radioactivity in the samples, respectively. The two metabolites co-eluted in the initial HPLC system (Figure 2A), however, when the second HPLC system was used, M20 and M24 were separated into two distinct chromatographic peaks in the MS extracted ion chromatogram (data not shown). M5 was the major metabolite in rat liver microsomes accounting for 37% of total radioactivity (Figure 2A). M4 and M6 were only detected in small amounts in all three species. Other microsomal metabolites included M3a, M3b, M7, M9, M23a,b, M28 a,b, and M29a,b. All of the metabolites that were detected in human microsomes were also formed in either rat or monkey liver microsomes.

Downloaded from dmd.aspetjournals.org at ASPET Journals on April 10, 2024

DMD Fast Forward. Published on April 17, 2008 as DOI: 10.1124/dmd.107.018234
This article has not been copyedited and formatted. The final version may differ from this version.

The primary oxidative metabolites identified in microsomes, namely, M4, M5, M6, M20 and M24, were also detected in hepatocyte incubations. Secondary metabolites, produced from further metabolism of these metabolites were observed in monkey and human (M7 and M23a,b). M21 and M30 (not detected in rat) were also identified. All metabolites that were detected in human hepatocytes were also formed either in rat or monkey hepatocytes.

Excretion of the Radioactive Dose: The recovery of radioactivity in the urine and bile of bile duct-cannulated rats and monkeys and in the urine and feces of intact rats and monkeys following administration of a single oral or IV dose of [^{14}C]dasatinib is summarized in Table 1. The excretion in the urine and feces in the 0-168 h interval after oral administration of dasatinib was 6.4% and 76.4% of the dose in intact rats and 3.0 and 76.8% of the dose in monkeys, respectively. In bile duct-cannulated monkeys, 9.9%, 67.2% and 13.7% of the dose was recovered in the urine, bile, and feces, respectively, in the 0-72 h interval after IV administration. The total recovery of the radioactive dose in these studies was >88% over the collection intervals. In bile duct-cannulated rats, 3.2 and 35.8% of the dose was excreted in the urine and bile of orally-dosed rats and 12.0 and 67.4% of the dose was excreted in the urine and bile of IV-dosed animals in the 0-12 h interval post-dose.

Plasma concentration profiles of radioactivity and dasatinib: The plasma concentration versus time pharmacokinetic (PK) profiles for total radioactivity (TRA) and dasatinib after administration of a single oral dose of [^{14}C]dasatinib to intact rat and monkey are presented in the upper panels of Figures 3 and 4, respectively. For both rat and monkey, the plasma concentration of TRA was significantly higher than the plasma

Downloaded from dmd.aspetjournals.org at ASPET Journals on April 10, 2024

DMD Fast Forward. Published on April 17, 2008 as DOI: 10.1124/dmd.107.018234
This article has not been copyedited and formatted. The final version may differ from this version.

concentration of dasatinib at all time points where there was measurable value for each (up to 8 h). The AUC (0-8 h) for TRA and dasatinib were 2183 and 1232 ng-h/mL in rats and 2076 and 545 ng-h/mL in monkeys, respectively. Based on these calculated exposures, dasatinib comprised approximately 56% and 26% of the AUC (0-8 h) of TRA, while metabolites accounted for about 44% and 74% of the AUC (0-8 h) of TRA in rats and monkeys, respectively.

Metabolite Profiles in Plasma: Representative metabolite profiles in extracts of pooled plasma samples collected 4 h after oral administration of [^{14}C]dasatinib to rats and monkeys are shown in the lower panels of Figures 3 and 4, respectively. At 4 h after dose administration, unchanged dasatinib (P) was the most abundant circulating component, representing approximately 53% and 32% of the plasma radioactivity in rats and monkeys, respectively (Table 2). In rat plasma, a piperazine *N*-oxide (M5) was the major circulating metabolite. Glucuronide (M8c) and sulfate (M13) conjugates of dasatinib were also prominent metabolites in rat. In monkey plasma, a glucuronide conjugate of dasatinib (M8a) was the most prominent metabolite, with multiple other minor metabolites detected as minor components. Plasma profiles from IV- or orally-dosed BDC rats were qualitatively similar to orally dosed intact rats, and the distribution of metabolites in the plasma samples analyzed at 1 and 8 h was similar to the 4-h samples (data not shown). For monkeys, only the 4-h plasma sample from the orally-dosed intact animals was analyzed; plasma samples collected after this time point did not contain enough radioactivity to generate a metabolic profile.

Metabolite Profiles in Bile: Biliary profiles of radioactivity indicated that dasatinib was extensively metabolized in both rats and monkeys. Representative radiochromatograms

Downloaded from dmd.aspetjournals.org at ASPET Journals on April 10, 2024

DMD Fast Forward. Published on April 17, 2008 as DOI: 10.1124/dmd.107.018234
This article has not been copyedited and formatted. The final version may differ from this version.

of pooled bile samples, collected for 0-12 h (rats) and 0-72 h (monkeys) after IV administration of [^{14}C]dasatinib are shown in the upper panels of Figure 5. The distribution of metabolites in bile profiles obtained from BDC rats administered an oral dose of [^{14}C]dasatinib were similar to the profile obtained from IV-dosed rats (data not shown). The concentrations of metabolites expressed as a percent of dose are summarized in Table 3. Unchanged dasatinib represented 11.1 and 3.2% of the dose in rats and monkeys, respectively. A piperazine *N*-oxide (M5), a carboxylic acid metabolite of dasatinib (M6) and a sulfate conjugate of phenyl-hydroxylated dasatinib (M21) were prominent metabolites common to both species. The other significant metabolites that were present in both rat and monkey bile were direct glucuronide conjugates of dasatinib (M8 in rat and M8a,b in monkey). In monkey bile, a mono-oxidation product of M6 (M7) was also a major biliary metabolite along with other significant secondary metabolites (M30, M31, M34 and M35b) that were not observed in rat bile.

Metabolite Profiles in Feces: The metabolite profiles of feces were qualitatively similar between rats and monkeys. Representative radiochromatograms of pooled feces samples collected in the 0-168 h interval after administration of an oral dose of [^{14}C]dasatinib are shown in lower panels of Figure 5. The distribution of radioactive components in the feces expressed as percent of dose excreted are detailed in Table 3. The parent compound in feces comprised 41.6% (rats) and 24.7% (monkeys) of the recovered dose. M4, M6, M7, M20, M24, M23a and M23b were identified in the feces samples from both species.

Metabolite Profiles in Urine: The predominant compound in both rat and monkey urine was M5 which comprised ≤ 3.4% of the dose (Table 3). Unchanged dasatinib was also a

Downloaded from dmd.aspetjournals.org at ASPET Journals on April 10, 2024

DMD Fast Forward. Published on April 17, 2008 as DOI: 10.1124/dmd.107.018234
This article has not been copyedited and formatted. The final version may differ from this version.

major urinary component (≤ 0.7% of the dose). Numerous minor metabolites were detected in the urine from both species.

Identification of Metabolites: The structures of metabolites were elucidated by LC/MS^2 or LC/MS^3 analysis and by comparison of chromatographic retention times and mass spectral fragmentation patterns to available reference standards. A listing of the metabolites of dasatinib detected in liver microsomes and hepatocytes from rat, monkey and human, and the *in vivo* samples from rats and monkeys treated with dasatinib is compiled in Table 4 along with the mass spectral fragmentation data supporting the identification of each of the metabolites. Proposed structures and metabolic pathways for the formation of the detected metabolites are shown in Figure 1.

Under positive ESI, dasatinib had a protonated molecular ion at *m/z* 488 with product ions at m/z 401, 347, 319, 260, and 232. The mass spectral fragmentation pattern for dasatinib, illustrated at the top of Table 4, showed cleavage across the piperazine ring resulting in a fragment ion at *m/z* 401, and cleavage at the carboxamide linkage, resulting in fragment ions at *m/z* 347 and 319. Further cleavage of *m/z* 401 produced fragment ions at *m/z* 260 and 232. High resolution mass spectral information for each of these major fragment ions supported the proposed fragmentation. The metabolites of dasatinib underwent similar fragmentations, enabling assignment and localization of metabolic transformations by comparison of changes in the masses of fragment ions relative to the parent molecule.

Metabolites M4, M5 and M6 were identified as *N*-dealkylated dasatinib (deshydroxyethyl), the piperazine *N*-oxide, and the carboxylic acid, respectively (Figure 1). These metabolites had the same retention time and mass spectral fragmentation

Downloaded from dmd.aspetjournals.org at ASPET Journals on April 10, 2024

DMD Fast Forward. Published on April 17, 2008 as DOI: 10.1124/dmd.107.018234
This article has not been copyedited and formatted. The final version may differ from this version.

patterns as chemically synthesized reference standards. The major MS^2 fragments and proposed MS fragmentation pattern for these metabolites are shown in Table 4. The MS^2 spectrum of the piperazine *N*-oxide (*m/z* 504) showed a neutral loss 44 Da (a vinyl alcohol), suggesting that the hydroxyethyl group was intact. The further loss of 33 Da from *m/z* 460 to *m/z* 427 (a possible hydroxylamine) indicated the formation of an *N*-oxide.

Metabolites M3a and M3b both had a protonated molecular ion at *m/z* 520 under positive full MS scans. M3a and M3b were detected as two peaks under the second set of HPLC conditions used for analysis of in vitro samples. The MS^2 spectra from both metabolites were nearly identical, except that M3b showed a greater propensity for loss of water upon activation in the mass spectrometer. Fragment ions at *m/z* 417 and 363 suggested that oxidation occurred on both the piperazine and the 2-chloro-6-methylphenyl moieties. The MS^2 spectrum of *m/z* 520 displayed similar neutral losses of 44 Da and 33 Da as the *N*-oxide metabolite, M5. Based on these data, M3a and M3b were tentatively identified as the positional isomers of 2-chloro-6-methylphenyl ring-hydroxylated derivatives of the *N*-oxide of dasatinib.

Metabolite M7 had a protonated molecular ion at *m/z* 518, which is 30 Da higher than the parent. The MS^2 of *m/z* 518 showed one major fragment ion at *m/z* 456, which could be formed through the loss of the elements of water and carbon dioxide. Further fragmentation of *m/z* 456 (MS^3) showed a major ion at *m/z* 401, suggesting that the modifications were on the hydroxyethyl piperazine moiety. M7 was tentatively identified as the *N*-oxide of the carboxylic acid metabolite of dasatinib.

Downloaded from dmd.aspetjournals.org at ASPET Journals on April 10, 2024

DMD Fast Forward. Published on April 17, 2008 as DOI: 10.1124/dmd.107.018234
This article has not been copyedited and formatted. The final version may differ from this version.

Metabolites M8, M8a, M8b, and M8c each had a protonated molecular ion at *m/z* 664. The MS^2 spectrum of *m/z* 664 showed one major fragment at *m/z* 488 (a neutral loss of 176 Da), indicative of a glucuronide conjugate. MS^3 analysis of *m/z* 488 showed a fragmentation pattern similar to that of dasatinib. These metabolites were tentatively identified as positional isomers of glucuronidated dasatinib.

Metabolite M9 showed a molecular ion at *m/z* 486, 2 Da lower than that of the parent. Fragment ions at *m/z* 347, 319, and 263 in the MS^2 spectrum (Figure 6A) suggested the loss of 2 protons occurred on the 2-chloro-6-methylphenyl carboxamide moiety. The base fragment ion at *m/z* 399 is also consistent with the assignment. In order to gain more structural information on M9, a monkey liver microsome incubation sample containing M9 was exposed to 1 N HCl (pH=2). A hydrated product was formed and the mass spectral information is consistent with a hydrated form of M9 (Figure 6B). The hydrated M9 decomposed with loss of 139 Da upon solvent evaporation to yield a product consistent with the formation of a carboxylic acid (*m/z* 365, Figure 6C). These observations are consistent with the proposed structure for M9 (Figure 1). Therefore, M9 was tentatively identified as a metabolite formed with an initial metabolism of the 2-chloro-6-methyl carboxamide moiety followed by formation of a new 6-membered ring.

Metabolite M13 had a molecular ion at *m/z* 568, which is 80 Da higher than that of the parent. The MS^2 spectrum of *m/z* 568 showed one major fragment at *m/z* 488 (a neutral loss of 80 Da), indicative of a glucuronide conjugate. MS^3 analysis of *m/z* 488 showed a fragmentation pattern similar to that of dasatinib. Based on these data, M13 was tentatively identified as a sulfate conjugate of dasatinib.

Downloaded from dmd.aspetjournals.org at ASPET Journals on April 10, 2024

DMD Fast Forward. Published on April 17, 2008 as DOI: 10.1124/dmd.107.018234
This article has not been copyedited and formatted. The final version may differ from this version.

Metabolite M14 had a molecular ion at *m/z* 462, which is 26 Da less than the parent. The MS^2 spectrum of *m/z* 462 showed fragment ions at 401, 375, and 321. MS^3 analysis of *m/z* 401 produced fragments at *m/z* 260, and 232, similar to dasatinib, suggesting that the loss of mass had occurred on the hydroxyethyl piperazine moiety. These data suggest that M14 is a secondary metabolite of dasatinib, formed via M4, through *N*-dealkylation of the piperazine ring, followed by oxidation of the resulting aldehyde to an alcohol.

Metabolite M15 had a molecular ion at m/z 520 (32 Da higher than dasatinib) and major MS^2 fragments at *m/z* 502 (loss of water), 401, and 379. The MS^3 analysis of *m/z* 401 produced fragments at *m/z* 260 and 232, similar to dasatinib. These data suggest that M15 is a bis-oxygenated metabolite of dasatinib, with the site of both additions on the hydroxyethyl piperazine moiety.

Metabolite M20 had a molecular ion of *m/z* 504, which is 16 Da higher than that of the parent. The MS^2 spectrum of *m/z* 504 showed the major fragment ion at *m/z* 417 and smaller ions at *m/z* 347 and 319, suggesting hydroxylation occurred on the 2-chloro-6-methylphenyl ring (Table 4, Top). In order to determine the exact site of hydroxylation, M20 was isolated from a large-scale human liver microsome incubation for NMR analysis (Table 5). The ^{1}H-NMR spectrum showed that the aromatic-CH_3 signal (δ 2.14 ppm) at C-7 was intact. The coupling pattern of protons on the 2-chloro-6-methylphenyl ring changed from a doublet-doublet-triplet pattern in dasatinib to a doublet-doublet pattern in M20, and the small coupling constant of 2.65 Hz in M20 implied a meta coupling. These data suggested that the hydroxylation occurred at the C-4 position. The structural assignment was consistent with the proton-carbon correlation pattern in the

Downloaded from dmd.aspetjournals.org at ASPET Journals on April 10, 2024

DMD Fast Forward. Published on April 17, 2008 as DOI: 10.1124/dmd.107.018234
This article has not been copyedited and formatted. The final version may differ from this version.

HMBC spectrum (Table 5). These results confirmed M20 as the 4-hydroxy-2-chloro-6-methylphenyl metabolite of dasatinib.

Metabolite M21 showed a molecular ion at *m/z* 584. The major fragment ion, *m/z* 504, in the MS^2 spectrum of *m/z* 584 suggested the loss of a sulfate group (80 Da). Further cleavage of *m/z* 504 generated ions at *m/z* 417 and 347. These data suggested that M21 is a sulfate conjugate of the phenyl ring-hydroxylated dasatinib. In an incubation of M20 with human liver cytosol in the presence of PAPS, a sulfate conjugate of M20 was detected using mass spectrometry (data not shown). The sulfate conjugate formed in cytosol displayed identical HPLC retention time and MS^2 fragment ions as those of metabolite M21. Therefore, M21 was identified as a sulfate conjugate of M20.

Metabolite M22 had a molecular ion at *m/z* 504. Major fragment ions of *m/z* 504 included ions at *m/z* 486, 401, and 375, indicating hydroxylation had occurred on the hydroxyethyl piperazine moiety.

Metabolites M23, M23a and M23b each had a molecular ion at *m/z* 518. The MS^2 spectra from these metabolites contained ions at *m/z* 417 and 361, suggesting hydroxylation on the 2-chloro-6-methylphenyl ring and formation of a carboxylic acid. A significant loss of water was observed for M23 and M23b. Based on this information, these metabolites were tentatively identified as the positional isomers of 2-chloro-6-methylphenyl ring-hydroxylated derivatives of the carboxylic acid metabolite.

Metabolite M24 showed a molecular ion of *m/z* 504. Major fragment ions of *m/z* 504 included ions at *m/z* 486, 417, and 347, indicating hydroxylation on the 2-chloro-6-methylphenyl ring (Table 4, Top). The significant loss of a molecule of water upon activation in the ion trap suggested the possible site of hydroxylation was on the methyl

Downloaded from dmd.aspetjournals.org at ASPET Journals on April 10, 2024

DMD Fast Forward. Published on April 17, 2008 as DOI: 10.1124/dmd.107.018234
This article has not been copyedited and formatted. The final version may differ from this version.

group. M24 was also isolated for NMR analysis and the results are shown in Table 5. In the proton NMR spectrum, the coupling pattern of protons on the 2-chloro-6-methylphenyl ring (δ 7.3-7.6 ppm) suggested that all three protons on the ring were intact. However, the 2.25 ppm singlet signal corresponding to the benzylic-CH_3 at the C-7 position in dasatinib disappeared and a new singlet appeared at 4.54 ppm, matching an ACD/NMR prediction for Ar-CH_2OH at the C-7 position (Table 5). Thus, the NMR data supported a structural assignment in which the hydroxylation was at the C-7. M24 was identified as the benzyl alcohol derivative of dasatinib.

Metabolite 26 had a molecular ion at *m/z* 609, 121 Da higher than dasatinib and major MS^2 fragments at *m/z* 468, 456, 444 and 401. The fragment at *m/z* 444, equivalent to M4, suggested that the piperazine ring was intact and that the hydroxyethyl group had been modified. These data support the conclusion that M26 is a taurine conjugate of dasatinib.

Metabolites M28a and M28b had the same molecular ion at *m/z* 460, 16 Da higher than that of *N*-dealkylated dasatinib (M4). Fragment ions at *m/z* 303 and 275 in the MS^2 spectra from both metabolites were consistent with *N*-dealkylation of the hydroxyethyl group, and a fragment ion at *m/z* 417 indicated hydroxylation on the 2-chloro-6-methylphenyl group. The degree of water loss and the intensity of fragment ion *m/z* 417 were the only differences observed in their MS^2 spectra (data not shown). M28a and M28b were tentatively identified as the positional isomers of 2-chloro-6-methylphenyl ring-hydroxylated M4.

Metabolites M29a, M29b, and M29c all showed a molecular ion at *m/z* 520 and were separated into three peaks under the first HPLC system used for analysis of the in

Downloaded from dmd.aspetjournals.org at ASPET Journals on April 10, 2024

DMD Fast Forward. Published on April 17, 2008 as DOI: 10.1124/dmd.107.018234
This article has not been copyedited and formatted. The final version may differ from this version.

vitro samples. The MS^2 spectra from the three metabolites all contained fragment ions at *m/z* 433 and 347, indicating two hydroxyl groups were added on the 2-chloro-6-methylphenyl moiety. MS^3 spectra obtained from further cleavage of *m/z* 433 were similar for all three metabolites, except a more significant water loss was observed for M29b. Based on these data, the three metabolites were tentatively identified as the positional isomers of dihydroxylated dasatinib, with both hydroxylations occurring on the 2-chloro-6-methylphenyl ring.

Metabolite M30 had a molecular ion at *m/z* 598. An ion at *m/z* 518 (loss of 80 Da, a sulfate group) was also observed in full MS scans, most likely due to the in source fragmentation of the molecular ion. Further cleavage of *m/z* 518 generated ions at *m/z* 417 and 361, indicating hydroxylation on the 2-chloro-6-methylphenyl ring and formation of a carboxylic acid. M30 was tentatively identified as the sulfate conjugate of the 2-chloro-6-methylphenyl ring-hydroxylated M6.

Metabolite M31 showed a molecular ion at *m/z* 600. Upon activation of *m/z* 600, the major fragment ion at *m/z* 520 was formed, indicating a loss of a sulfate group. MS^3 spectrum of *m/z* 520 contained ions at *m/z* 433 and 347, indicating bis-hydroxylation on the 2-chloro-6-methylphenyl ring. Therefore, M31 was tentatively identified as a sulfate conjugate of one of the dihydroxylated dasatinib isomers.

Metabolite M34 showed a molecular ion at *m/z* 534. MS^2 fragment ions at *m/z* 377 and 333 suggested the formation of a carboxylic acid and *N*-oxidation of the piperazine ring, while MS^2 fragment ions at *m/z* 472 and 403 indicated hydroxylation on the 2-chloro-6-methylphenyl ring. These data suggest that M34 is a metabolite that has undergone 3 oxidations including: hydroxylation of the 2-chloro-6-methylphenyl ring, *N*-

Downloaded from dmd.aspetjournals.org at ASPET Journals on April 10, 2024

DMD Fast Forward. Published on April 17, 2008 as DOI: 10.1124/dmd.107.018234
This article has not been copyedited and formatted. The final version may differ from this version.

oxidation of the piperazine ring, and oxidation of the hydroxyethyl group to a carboxylic acid.

Metabolite M35a and M35b each showed a molecular ion at *m/z* 662. The MS^2 spectra of both metabolites contained a fragment ion at *m/z* 486, a neutral loss of 176, indicative of a glucuronide conjugate. The MS^3 spectrum of *m/z* 486 showed a fragmentation pattern similar to that of M9, with ions at *m/z* 399, 347, and 263. Based on these data, M35a and M35b were tentatively identified as positional isomers of glucuronidated dehydrogenated dasatinib.

Metabolite M36 showed a molecular ion at *m/z* 694. The MS^2 spectra of *m/z* 694 contained a major fragment ion at *m/z* 518. The neutral loss of 176 Da from 694, indicated that M36 was a glucuronide conjugate. Further fragmentation of *m/z* 518 included ions at *m/z* 417 and 361, indicating hydroxylation on the 2-chloro-6-methylphenyl ring and formation of a carboxylic acid. Therefore, M36 was tentatively identified as a glucuronide of the 2-chloro-6-methylphenyl ring hydroxylated, carboxylic acid derivative of dasatinib.

Metabolites M37a and M37b both showed a molecular ion at *m/z* 680. The MS^2 spectra of *m/z* 680 contained a major fragment ion at *m/z* 504 (neutral loss of 176 Da) indicating that these metabolites were glucuronide conjugates. The MS^3 spectrum of *m/z* 504 showed fragment ions at *m/z* 417 and 347, suggesting hydroxylation on the 2-chloro-6-methylphenyl ring. A significant loss of water (*m/z* 486) was observed for M37b, indicating that the site of hydroxylation for this metabolite was likely to be on the methyl group. Based on these data, M37a and M37b were tentatively identified as positional isomers of glucuronidated 2-chloro-6-methylphenyl ring hydroxylated dasatinib.

Downloaded from dmd.aspetjournals.org at ASPET Journals on April 10, 2024

DMD Fast Forward. Published on April 17, 2008 as DOI: 10.1124/dmd.107.018234
This article has not been copyedited and formatted. The final version may differ from this version.

Formation of M6 in Human Liver Cytosol Fraction: HPLC-MS analysis showed that metabolite M6 was formed from dasatinib in incubations of human liver cytosol in the presence of cofactor NAD^+ or $NADP^+$ (data not shown). Figure 7 shows the relative formation of M6 in vitro in human liver tissue fractions under various incubation conditions. A minimal amount of M6 was produced when dasatinib was incubated with human liver cytosol or microsomes without the addition of cofactors. Formation of M6 was approximately 5-fold higher in human liver cytosol in the presence of NAD^+ than in microsomal incubations in the presence of NADPH (Figure 7). M6 was produced in human liver cytosol fractions when either NAD^+ or $NADP^+$ was used as the cofactor. 4-Methylpyrazole (100 μM), an inhibitor of alcohol dehydrogenase (Walsh et al., 2002) and disulfiram, an inhibitor of aldehyde dehydrogenase (Lipsky et al., 2001) reduced M6 formation by 88 and 67%, respectively (Figure 7).

Downloaded from dmd.aspetjournals.org at ASPET Journals on April 10, 2024

DMD Fast Forward. Published on April 17, 2008 as DOI: 10.1124/dmd.107.018234
This article has not been copyedited and formatted. The final version may differ from this version.

DISCUSSION

A relatively high dasatinib turnover rate was observed in liver microsomes from all three species, with monkey liver microsomes showing the highest turnover and rat the lowest (Figure 2A). A similar trend was observed in hepatocytes from all three species (Figure 2B). Although no effort was made to optimize the incubation conditions, these results are consistent with previous in vivo pharmacokinetic studies which showed a moderate systemic plasma clearance of dasatinib in rats (26 mL/min/kg, 47% hepatic blood flow) after an intra-arterial dose, and a high clearance in monkeys (34 mL/min/kg, 77% hepatic blood flow) after an intravenous dose (Kamath et al., 2008).

Species differences in the metabolism of dasatinib were observed in the *in vitro* incubations. The *N*-oxide (M5) was the most abundant metabolite in rat liver microsomes, whereas, metabolites M20 and M24 were the most abundant components in monkey and human liver microsomes (Figure 2A). Similarly, metabolites M20, M24 and the sulfate of M20 were the prominent metabolites in monkey and human hepatocytes, while M5 and M6 were the most abundant metabolites in rat hepatocytes.

Following administration of a single oral dose of [^{14}C]dasatinib to intact rats and monkeys, the majority of the radioactivity (>76%) was excreted in feces and only a small portion (<7%) was recovered in urine (Table 1). Similarly, after IV administration of [^{14}C]dasatinib to BDC rats and monkeys, the majority of the radioactive dose was excreted in bile (~67%). After IV administration of [^{14}C]dasatinib to BDC monkeys, 13.7% of the dose was recovered in the feces, suggesting intestinal secretion of drug-derived radioactivity. Since feces samples were not collected from BDC rats, intestinal secretion in rats cannot be evaluated from the current experiments. However, prior

Downloaded from dmd.aspetjournals.org at ASPET Journals on April 10, 2024

DMD Fast Forward. Published on April 17, 2008 as DOI: 10.1124/dmd.107.018234
This article has not been copyedited and formatted. The final version may differ from this version.

studies in BDC rats indicated that 3.5% of the dose was secreted as parent in the GI tract (Kamath et al., 2008) after IV administration of unlabeled dasatinib. Furthermore, bidirectional permeability studies with Caco-2 cell monolayers suggested that dasatinib could be a substrate for efflux transporters (Kamath et al., 2008). Taken together, these data suggest that efflux transporters may play a role in the disposition of dasatinib.

Plasma PK profiles of TRA and dasatinib (Figures 3 and 4, upper panels) suggested that metabolites contributed significantly to the AUC of TRA. These data are consistent with the metabolite profiles from the 4-h rat and monkey plasma samples (Table 2, Figures 3 and 4, lower panels), which showed that dasatinib was the major circulating component, while multiple metabolites contributed to the remaining 40-60% of the sample radioactivity at that time point. In both rat and monkey, multiple oxidative and conjugative metabolites were detected in the plasma. In rat, the major circulating metabolite was the piperazine *N*-oxide (M5), along with glucuronide (M8c) and sulfate (M13) conjugates of dasatinib. Whereas, in monkey, a glucuronide conjugate of dasatinib (M8a) and a sulfate conjugate of mono-hydroxylated M6 (M30) were the most prominent plasma metabolites; multiple additional metabolites each comprised <5% of the sample radioactivity. The rat and monkey plasma profiles were qualitatively similar to the hepatocyte profiles in the respective species.

Earlier work with unlabeled dasatinib suggested that it was extensively metabolized and excreted mainly in the bile (Kamath et al., 2008). Therefore, the current studies with [^{14}C]-labeled dasatinib were conducted in both intact and BDC animals to understand the role of oxidative and conjugative metabolism in the disposition of the compound and to provide a quantitative estimate of the various drug-related species in

Downloaded from dmd.aspetjournals.org at ASPET Journals on April 10, 2024

DMD Fast Forward. Published on April 17, 2008 as DOI: 10.1124/dmd.107.018234
This article has not been copyedited and formatted. The final version may differ from this version.

bile, feces and urine. After oral administration of [^{14}C]dasatinib to rats and monkeys, <12% of the dose was excreted as unchanged dasatinib in bile and <1% was excreted in the urine (Table 3), indicating that the drug was extensively metabolized in the two species. In both species, a large portion of the radioactivity excreted in the bile (>29% of the dose) was attributed to *N*-oxides and conjugated metabolites. In contrast, in the feces of intact animals dosed orally with [^{14}C]dasatinib, most of the excreted dose was attributed to dasatinib and oxidative metabolites other than *N*-oxides. The striking difference in the bile and fecal profiles (Figure 5) can be explained by the hydrolysis of the conjugative metabolites (glucuronide and sulfate conjugates) and reduction of *N*-oxide metabolites during their passage through the GI tract prior to excretion in the feces. Hydrolysis or reduction by the GI gut flora has been reported for a number of conjugates and *N*-oxide metabolites (Parker et al., 1980; Jaworski et al., 1991; Mitchell et al., 1997; Slatter et al., 2000). These differences in the bile and fecal profiles for dasatinib exemplify the utility of BDC animals studies in the understanding the complete ADME profile of a drug. In the absence of BDC study, it may have been erroneously concluded that the presence of dasatinib in feces was due to incomplete absorption or direct excretion of the parent compound into the bile.

The proposed metabolic scheme for the biotransformation of dasatinib in rat, monkey and human is shown in Figure 1. Overall, the in vitro metabolic pathways of dasatinib involved: 1) hydroxylation on the 2-chloro-6-methylphenyl ring to form regio-isomeric metabolites M20 and M24; 2) *N*-dealkylation leading to loss of the hydroxyethyl group (M4); 3) piperazine *N*-oxidation (M5); 4) oxidation of the terminal alcohol to a carboxylic acid (M6); and 5) direct glucuronidation or sulfate conjugation of dasatinib.

Downloaded from dmd.aspetjournals.org at ASPET Journals on April 10, 2024

DMD Fast Forward. Published on April 17, 2008 as DOI: 10.1124/dmd.107.018234
This article has not been copyedited and formatted. The final version may differ from this version.

A unique dehydrogenated metabolite of dasatinib, M9, was detected in monkey and human liver microsomal incubations and in monkey feces. The loss of two protons was proposed to have occurred on the 2-chloro-6-methylphenyl carboxamide moiety followed by formation of a new 6-membered ring (Figure 6). Since the postulated structure of M9 contained an imine moiety, the acid stability of the product was tested. The product was susceptible to the formation of a carbinolamine (hydrated M9) under acid conditions (Figure 6B) and further decomposed to a carboxylic acid derivative. A similar reaction has been reported in the metabolism of trazodone (Kalgutkar et al., 2005). The scheme for the decomposition of M9 under acidic conditions is shown in Figure 6C. On the basis of these findings, a ring-closed structure on the 2-chloro-6-methylphenyl carboxamide moiety was proposed. Formation of M9 in liver microsomes required the presence of NADPH; M9 was not formed when metabolite M24 (a benzyl alcohol on the 2-chloro-6-methylphenyl ring, Figure 1) was incubated under various pH conditions. Detailed mechanisms involved in the formation of M9 remain to be examined.

The sulfate conjugation of hydroxylated metabolites M20 (4-hydroxy-2-chloro-6-methylphenyl) and M24 (7-hydroxy-2-chloro-6-methylphenyl) was investigated in human liver cytosol fractions. In the presence of PAPS, M20 was metabolized to form a sulfate conjugate, M21; M24 was not metabolized (data not shown). These results demonstrated regioselectivity in the sulfation of dasatinib and its hydroxylated metabolites, where formation of a phenol sulfate was preferred to a benzylic alcohol sulfate. Several examples of regioselectivity of sulfation have been published (Cui et al.,

Downloaded from dmd.aspetjournals.org at ASPET Journals on April 10, 2024

DMD Fast Forward. Published on April 17, 2008 as DOI: 10.1124/dmd.107.018234
This article has not been copyedited and formatted. The final version may differ from this version.

2004; Nakano et al., 2004), and human sulfotransferases 1E1, 1A3 and 1A1 have been shown to catalyze these reactions.

The carboxylic acid metabolite of dasatinib (M6) was detected in higher amounts in hepatocytes than in liver microsomal incubations for all three species (Figure 2), suggesting possible involvement of cytosolic enzymes in the formation of this metabolite. Incubations with microsomes in the presence of NADPH and cytosol in the presence of NAD^+ or $NADP^+$ were conducted to evaluate the involvement of cytosolic dehydrogenases (Figure 7) in the formation of M6. Inhibition of M6 formation by 4-methylpyrazole, an inhibitor of alcohol dehydrogenases (Boyer and Petersen, 1991), and by disulfiram, an inhibitor of aldehyde dehydrogenases (Boyer and Petersen, 1991), confirmed the involvement of these cytosolic enzymes in the production of M6. The involvement of alcohol and aldehyde dehydrogenases in the metabolism of xenobiotics has been well-documented (Walsh et al., 2002; Crabb et al., 2004; Vasiliou et al., 2004). In the current study, we confirmed that oxidation by cytosolic dehydrogenases to form M6 is one of the primary clearance pathways for dasatinib. The role of specific CYP and FMO enzymes in the oxidation of dasatinib will be described elsewhere.

In summary, data have been presented describing the in vitro metabolism of dasatinib in liver microsomes and hepatocytes from rat, monkey, and human. The in vitro metabolite profiles were qualitatively similar between the three species, although species differences in the major metabolic pathways were observed. The human metabolic profiles of dasatinib in both liver microsomes and hepatocytes closely resembled the monkey profiles. The major pathways for metabolism of dasatinib in rats and monkeys observed in vitro, were also prominent pathways for these species in vivo. Dasatinib was

Downloaded from dmd.aspetjournals.org at ASPET Journals on April 10, 2024

DMD Fast Forward. Published on April 17, 2008 as DOI: 10.1124/dmd.107.018234
This article has not been copyedited and formatted. The final version may differ from this version.

extensively metabolized in rats and monkeys with biliary excretion being the major route of elimination. Based on these data it is predicted that dasatinib will also be extensively metabolized in humans prior to elimination. The disposition of dasatinib in humans is the subject of a separate manuscript (Christopher et al., 2008).

ACKNOWLEDGMENTS: We would like to thank Dr. Feng Qiu (Bristol-Myers Squibb) for support in the NMR analysis and Dr. Qian Ruan (Bristol Myers Squibb) for helpful discussions.

Downloaded from dmd.aspetjournals.org at ASPET Journals on April 10, 2024

DMD Fast Forward. Published on April 17, 2008 as DOI: 10.1124/dmd.107.018234
This article has not been copyedited and formatted. The final version may differ from this version.

References

Allentoff AJ, Michael LW, Ogan M, Chen BC, Zhao R, Iyer RA, Christopher LJ, Rinehart JK, Balasubramanian B and Bonacorsi S (2008) Synthesis of ^{14}C-labeled and ^{13}C,^{15}N-labeled dasatinib and its piperazine N-dealkyl metabolite. *Journal of Labelled Compound and radiopharmaceuticals* **5:**41-47.

Boyer CS and Petersen DR (1991) The metabolism of 3,7-dimethyl-2,6-octadienal (citral) in rat hepatic mitochondrial and cytosolic fractions. Interactions with aldehyde and alcohol dehydrogenases. *Drug Metab Dispos* **19:**81-86.

Christopher LJ, Cui D, Wu C, Luo R, Manning JA, Bonacorsi SJ, Lago M, Allentoff AJ, Lee FYF, McCann B, Galbriath S, He K, Barros AJ, Blackwood-Chirchir A, Humphreys GW and Iyer RA (2008) Metabolism and Disposition of Dasatinib after Oral Administration to Humans. *Drug Metab Dispos* (In press DMD #018267).

Crabb DW, Matsumoto M, Chang D and You M (2004) Overview of the role of alcohol dehydrogenase and aldehyde dehydrogenase and their variants in the genesis of alcohol-related pathology. *Proc Nutr Soc* **63:**49-63.

Cui D, Booth-Genthe CL, Carlini E, Carr B and Schrag ML (2004) Heterotropic modulation of sulfotransferase 2A1 activity by celecoxib: product ratio switching of ethynylestradiol sulfation. *Drug Metab Dispos.* **32:**1260-1264.

Das J, Chen P, Norris D, Padmanabha R, Lin J, Moquin RV, Shen Z, Cook LS, Doweyko AM, Pitt S, Pang S, Shen DR, Fang Q, de Fex HF, McIntyre KW, Shuster DJ, Gillooly KM, Behnia K, Schieven GL, Wityak J and Barrish JC (2006) 2-aminothiazole as a novel kinase inhibitor template. Structure-activity relationship

Downloaded from dmd.aspetjournals.org at ASPET Journals on April 10, 2024

DMD Fast Forward. Published on April 17, 2008 as DOI: 10.1124/dmd.107.018234
This article has not been copyedited and formatted. The final version may differ from this version.

studies toward the discovery of N-(2-chloro-6-methylphenyl)-2-[[6-[4-(2-hydroxyethyl)-1- piperazinyl)]-2-methyl-4-pyrimidinyl]amino)]-1,3-thiazole-5-carboxamide (dasatinib, BMS-354825) as a potent pan-Src kinase inhibitor. *J Med Chem.* **49:**6819-6832.

de Graaf IAM, van Meijeren CE, Pektas F and Koster HJ (2002) Comparison of in Vitro Preparations for Semi-Quantitative Prediction of in Vivo Drug Metabolism. *Drug Metab Dispos* **30:**1129-1136.

Fricker J (2006) Beyond Gleevec--the next generation in CML. *Eur J Cancer.* **42:**275.

Hampton T (2006) Looking beyond imatinib: next line of targeted drugs for CML shows promise. *Jama.* **295:**369-370.

Hewitt NJ, Buhring KU, Dasenbrock J, Haunschild J, Ladstetter B and Utesch D (2001) Studies comparing in vivo:in vitro metabolism of three pharmaceutical compounds in rat, dog, monkey, and human using cryopreserved hepatocytes, microsomes, and collagen gel immobilized hepatocyte cultures. *Drug Metab Dispos.* **29:**1042-1050.

Jaworski TJ, Hawes EM, Hubbard JW, McKay G and Midha KK (1991) The metabolites of chlorpromazine N-oxide in rat bile. *Xenobiotica.* **21:**1451-1459.

Johnson FM, Saigal B, Talpaz M and Donato NJ (2005) Dasatinib (BMS-354825) tyrosine kinase inhibitor suppresses invasion and induces cell cycle arrest and apoptosis of head and neck squamous cell carcinoma and non-small cell lung cancer cells. *Clin Cancer Res.* **11:**6924-6932.

Kalgutkar AS, Henne KR, Lame ME, Vaz AD, Collin C, Soglia JR, Zhao SX and Hop CE (2005) Metabolic activation of the nontricyclic antidepressant trazodone to

Downloaded from dmd.aspetjournals.org at ASPET Journals on April 10, 2024

DMD Fast Forward. Published on April 17, 2008 as DOI: 10.1124/dmd.107.018234
This article has not been copyedited and formatted. The final version may differ from this version.

electrophilic quinone-imine and epoxide intermediates in human liver microsomes and recombinant P4503A4. *Chem Biol Interact* **155:**10-20.

Kamath AV, Wang J, Lee FY and Marathe PH (2008) Preclinical pharmacokinetics and in vitro metabolism of dasatinib (BMS-354825): a potent oral multi-targeted kinase inhibitor against SRC and BCR-ABL. *Cancer Chemother Pharmacol* **61:**365-376.

Li AP (2004) In vitro approaches to evaluate ADMET drug properties. *Curr Top Med Chem* **4:**701-706.

Li AP, Lu C, Brent JA, Pham C, Fackett A, Ruegg CE and Silber PM (1999) Cryopreserved human hepatocytes: characterization of drug-metabolizing enzyme activities and applications in higher throughput screening assays for hepatotoxicity, metabolic stability, and drug-drug interaction potential. *Chem Biol Interact* **121:**17-35.

Lin J, Sahakian DC, de Morais SM, Xu JJ, Polzer RJ and Winter SM (2003) The role of absorption, distribution, metabolism, excretion and toxicity in drug discovery. *Curr Top Med Chem* **3:**1125-1154.

Lipsky JJ, Shen ML and Naylor S (2001) In vivo inhibition of aldehyde dehydrogenase by disulfiram. *Chem Biol Interact* **130-132:**93-102.

Lombardo LJ, Lee FY, Chen P, Norris D, Barrish JC, Behnia K, Castaneda S, Cornelius LA, Das J, Doweyko AM, Fairchild C, Hunt JT, Inigo I, Johnston K, Kamath A, Kan D, Klei H, Marathe P, Pang S, Peterson R, Pitt S, Schieven GL, Schmidt RJ, Tokarski J, Wen ML, Wityak J and Borzilleri RM (2004) Discovery of N-(2-chloro-6-methyl-phenyl)-2-(6-(4-(2-hydroxyethyl)-piperazin-1-yl)-2-methyl

Downloaded from dmd.aspetjournals.org at ASPET Journals on April 10, 2024

DMD Fast Forward. Published on April 17, 2008 as DOI: 10.1124/dmd.107.018234
This article has not been copyedited and formatted. The final version may differ from this version.

pyrimidin-4- ylamino)thiazole-5-carboxamide (BMS-354825), a dual Src/Abl kinase inhibitor with potent antitumor activity in preclinical assays. *J Med Chem.* **47:**6658-6661.

Manley PW, Cowan-Jacob SW and Mestan J (2005) Advances in the structural biology, design and clinical development of Bcr-Abl kinase inhibitors for the treatment of chronic myeloid leukaemia. *Biochim Biophys Acta.* **1754:**3-13.

Mitchell SC, Zhang AQ, Noblet JM, Gillespie S, Jones N and Smith RL (1997) Metabolic disposition of [^{14}C]-trimethylamine N-oxide in rat: variation with dose and route of administration. *Xenobiotica.* **27:**1187-1197.

Nakano H, Ogura K, Takahashi E, Harada T, Nishiyama T, Muro K, Hiratsuka A, Kadota S and Watabe T (2004) Regioselective monosulfation and disulfation of the phytoestrogens daidzein and genistein by human liver sulfotransferases. *Drug Metab Pharmacokinet.* **19:**216-226.

Naritomi Y, Terashita S, Kagayama A and Sugiyama Y (2003) Utility of hepatocytes in predicting drug metabolism: comparison of hepatic intrinsic clearance in rats and humans in vivo and in vitro. *Drug Metab Dispos* **31:**580-588.

O'Hare T, Walters DK, Stoffregen EP, Jia T, Manley PW, Mestan J, Cowan-Jacob SW, Lee FY, Heinrich MC, Deininger MW and Druker BJ (2005) In vitro activity of Bcr-Abl inhibitors AMN107 and BMS-354825 against clinically relevant imatinib-resistant Abl kinase domain mutants. *Cancer Res.* **65:**4500-4505.

Pang KS, Barker F, Simard A, Schwab AJ and Goresky CA (1995) Sulfation of acetaminophen by the perfused rat liver: the effect of red blood cell carriage. *Hepatology* **22:**267-282.

Downloaded from dmd.aspetjournals.org at ASPET Journals on April 10, 2024

DMD Fast Forward. Published on April 17, 2008 as DOI: 10.1124/dmd.107.018234
This article has not been copyedited and formatted. The final version may differ from this version.

Parker RJ, Hirom PC and Millburn P (1980) Enterohepatic recycling of phenolphthalein, morphine, lysergic acid diethylamide (LSD) and diphenylacetic acid in the rat. Hydrolysis of glucuronic acid conjugates in the gut lumen. *Xenobiotica.* **10:**689-703.

Roberts SA (2003) Drug metabolism and pharmacokinetics in drug discovery. *Curr Opin Drug Discov Devel.* **6:**66-80.

Schittenhelm MM, Shiraga S, Schroeder A, Corbin AS, Griffith D, Lee FY, Bokemeyer C, Deininger MW, Druker BJ and Heinrich MC (2006) Dasatinib (BMS-354825), a dual SRC/ABL kinase inhibitor, inhibits the kinase activity of wild-type, juxtamembrane, and activation loop mutant KIT isoforms associated with human malignancies. *Cancer Res.* **66:**473-481.

Shah NP, Tran C, Lee FY, Chen P, Norris D and Sawyers CL (2004) Overriding imatinib resistance with a novel ABL kinase inhibitor. *Science.* **305:**399-401.

Slatter JG, Schaaf LJ, Sams JP, Feenstra KL, Johnson MG, Bombardt PA, Cathcart KS, Verburg MT, Pearson LK, Compton LD, Miller LL, Baker DS, Pesheck CV and Lord RS, III (2000) Pharmacokinetics, Metabolism, and Excretion of Irinotecan (CPT-11) Following I.V. Infusion of [^{14}C]CPT-11 in Cancer Patients. *Drug Metab Dispos* **28:**423-433.

Vasiliou V, Pappa A and Estey T (2004) Role of human aldehyde dehydrogenases in endobiotic and xenobiotic metabolism. *Drug Metab Rev* **36:**279-299.

Walsh JS, Reese MJ and Thurmond LM (2002) The metabolic activation of abacavir by human liver cytosol and expressed human alcohol dehydrogenase isozymes. *Chem Biol Interact* **142:**135-154.

Downloaded from dmd.aspetjournals.org at ASPET Journals on April 10, 2024

DMD Fast Forward. Published on April 17, 2008 as DOI: 10.1124/dmd.107.018234
This article has not been copyedited and formatted. The final version may differ from this version.

Zhu M, Zhao W, Vazquez N and Mitroka JG (2005) Analysis of low level radioactive metabolites in biological fluids using high-performance liquid chromatography with microplate scintillation counting: method validation and application. *J Pharm Biomed Anal.* **39:**233-245.

Downloaded from dmd.aspetjournals.org at ASPET Journals on April 10, 2024

DMD Fast Forward. Published on April 17, 2008 as DOI: 10.1124/dmd.107.018234
This article has not been copyedited and formatted. The final version may differ from this version.

Footnote

[*]**Send Reprint Request to:** Ramaswamy A. Iyer, Ph.D., Department of Biotransformation, Bristol-Myers Squibb Pharmaceutical Research Institute, P. O. Box 4000, Mail Stop F13-01, Princeton, NJ 08540.

[1]These authors contributed equally to the work.

[2]**Current Address:** Department of Drug Metabolism, Mail Stop WP75-100, Merck and Co., Inc., Sumneytown Pike , West Point, PA 19486.

Downloaded from dmd.aspetjournals.org at ASPET Journals on April 10, 2024

DMD Fast Forward. Published on April 17, 2008 as DOI: 10.1124/dmd.107.018234
This article has not been copyedited and formatted. The final version may differ from this version.

FIGURE LEGENDS

Figure 1 Proposed biotransformation pathways of dasatinib in rats, monkeys and humans. Pathways were proposed based on metabolites identified in *in vitro* incubations of [^{14}C]dasatinib with liver microsomes and hepatocytes from rat, monkey and human, and *in vivo* plasma, bile, urine and fecal samples collected from rats and monkeys administered a single dose of [^{14}C]dasatinib.

Figure 2 Representative radioactivity profiles of metabolites of [^{14}C]dasatinib (20 μM) in liver microsome (A) and hepatocyte incubations (B).

Figure 3 Plasma concentration of total radioactivity (TRA) and dasatinib versus time (top panel) and the biotransformation profile in the 4 h plasma sample (bottom panel) after oral administration of dasatinib to rats. The samples for TRA and the biotransformation profile were collected in a study where [^{14}C]dasatinib (10 mg/kg) was administered as a single oral dose to intact rats. The dasatinib versus time profile was generated from samples collected as part of a separate toxicokinetic (TK) study where rats were administered a single oral dose of non-radiolabeled dasatinib (10 mg/kg). The biotransformation profile (bottom panel) is a background subtracted reconstructed radiochromatogram of 15-sec fractions collected from an HPLC run.

Figure 4 Plasma concentration of total radioactivity (TRA) and dasatinib versus time (top panel) and the biotransformation profile in the 4 h plasma sample (bottom panel) after oral administration of dasatinib to monkeys.

Downloaded from dmd.aspetjournals.org at ASPET Journals on April 10, 2024

DMD Fast Forward. Published on April 17, 2008 as DOI: 10.1124/dmd.107.018234
This article has not been copyedited and formatted. The final version may differ from this version.

The samples for TRA and the biotransformation profile were collected in a study where [^{14}C]dasatinib (10 mg/kg) was administered as a single oral dose to intact monkeys. The dasatinib versus time profile was generated from samples collected as part of a separate toxicokinetic (TK) study where monkeys were administered a single oral dose of dasatinib (10 mg/kg). At 12 h, the concentration of radioactivity was below the lower limit of quantification. The biotransformation profile (bottom panel) is a background subtracted reconstructed radiochromatogram of 15-sec fractions collected from an HPLC run.

Figure 5 Biotransformation profiles in pooled bile (top panels) and fecal (bottom panels) samples from rat and monkey after a single dose of [^{14}C]dasatinib. The bile profiles are from IV-dosed rat and monkey and the fecal profiles are from orally dosed rat and monkey. The profiles are background subtracted reconstructed radiochromatograms of 15-sec fractions collected from an HPLC run.

Figure 6 (A) MS^2 product ion spectrum of M9 (MH^+ = 486) obtained on an ion-trap mass spectrometer. (B) MS^2 product ion spectrum of hydrated M9 under acidic conditions. (C) A scheme showing the proposed hydration and degradation of M9 to a carboxylic acid.

Figure 7 Formation of M6 in human in vitro matrices under various incubation conditions.

Downloaded from dmd.aspetjournals.org at ASPET Journals on April 10, 2024

TABLE 1

Percentage of dose recovered following administration of a single oral or IV dose of [^{14}C]dasatinib to rats and monkeys

Species	Route (Dose)	Collection Interval (h)	Percentage of Dose Recovered (mean ± S.D.)				
			Urine	Bile	Feces	Cage Debris /Wash	Total
Intact Rat (n=3)	Oral 15 mg/kg	0-168	6.45 ± 0.82	N.A.	76.39 ± 8.45	6.70 ± 4.88	89.54 ± 4.73
BDC Rat [a] (n=2)	Oral 10 mg/kg	0-12	3.2 (2.7, 3.6)	35.8 (32.5, 39.1)	N.C.	N.C.	39.0 [b] (35.2, 42.7)
BDC Rat [a] (n=2)	IV 10 mg/kg	0-12	12.0 (14.9, 9.1)	67.4 (61.2, 73.6)	N.C.	N.C.	79.4 (76.1, 82.7)
Intact monkey (n=3)	Oral 10 mg/kg	0-168	2.99 ± 1.55	N.A.	76.82 ± 9.75	8.84 ± 8.62	88.65 ± 2.42
BDC monkey (n=3)	IV 2 mg/kg	0-72	9.89 ± 2.88	67.24 ± 16.40	13.67 ± 12.66	N.C.	90.80 ± 2.56

N.A., not applicable; N.C., not collected.

[a] The BDC rat study was not run as a comprehensive mass-balance study; samples were only collected over a 12-h period. Since there were only two animals per treatment group, the standard deviation was not reported. The mean and individual recoveries for each animal were reported.

[b] An additional 61.2 (Rat 1) and 44.7% (Rat 2) of the radioactive dose was recovered in the GI tract of orally-dosed animals at the end of the study (12 h after drug administration), bringing the mean total recovery of radioactivity to 92.0%.

Downloaded from dmd.aspetjournals.org at ASPET Journals on April 10, 2024

DMD Fast Forward. Published on April 17, 2008 as DOI: 10.1124/dmd.107.018234
This article has not been copyedited and formatted. The final version may differ from this version.

DMD Fast Forward. Published on April 17, 2008 as DOI: 10.1124/dmd.107.018234
This article has not been copyedited and formatted. The final version may differ from this version.

TABLE 2

Relative abundance of dasatinib and metabolites in pooled plasma samples collected 4 h after administration of a single oral dose of [^{14}C]dasatinib to rats and monkeys

Metabolite ID	Percent of Sample Radioactivity	
	Rat	Monkey
M3a, M3b [a]	-	1.4
M4	2.6	3.0
M5	18.7	2.6
M6	2.2	2.7
M7	-	2.1
M8a	-	12.8
M8b, M23a, M23b [a, b]	-	4.5
M8c, M13 [c]	17.6	-
M20	-	2.8
M21	-	4.7
M24	-	0.7
M30	-	9.7
M31	-	1.7
M34	-	1.4
M35a	-	MS [d]
M37a, M37b [a]	-	3.7
Dasatinib	52.8	32.1

[a] Metabolites (M3a,b), (M23a,b), and (M37a,b) were pairs of positional isomers that were not well-resolved from each other chromatographically. The values reported represent the combined percentage for the co-eluting isomers.

[b] In monkey plasma metabolites M8b, M23a and M23b co-eluted.

[c] In rat plasma metabolites M8c and M13 co-eluted.

[d] In monkey plasma, metabolite M35a was detected by mass-spectrometry, but not by radioactivity.

Downloaded from dmd.aspetjournals.org at ASPET Journals on April 10, 2024

DMD Fast Forward. Published on April 17, 2008 as DOI: 10.1124/dmd.107.018234
This article has not been copyedited and formatted. The final version may differ from this version.

TABLE 3

Percentage of dose excreted as dasatinib and metabolites in pooled bile after administration of a single IV dose of [^{14}C]dasatinib to BDC rats and monkeys and in pooled feces and urine after administration of a single oral dose of [^{14}C]dasatinib to intact rats and monkeys

Metabolite ID	Percentage of Dose					
	Bile		Feces		Urine	
	Rat [a] (0-12 h)	Monkey [b] (0-72 h)	Rat [c] (0-168 h)	Monkey [c] (0-168 h)	Rat [c] (0-168 h)	Monkey [c] (0-168 h)
M3a, M3b [d]	-	2.0	-	-	0.1	0.1
M5	16.6	5.0	-	-	3.4	1.1
M4	14.1 [e]	0.5	1.9	2.9	0.3	0.05
M6		6.3	13.2	14.0	0.4	0.06
M7	-	8.3	0.8	0.4	0.02	0.3
M8	3.8	-	-	-	-	-
M8a	-	0.9	-	-	0.06	0.04
M8b	1.3 [f]	3.1 [g]	-	-	0.05	0.07
M23, M23a, M23b [d]			2.9	9.7	-	-
M9	-	-	-	1.3	-	-
M14	0.9	-	-	-	-	-
M15	0.8	-	-	-	-	-
M20	-	2.4	7.6	11.7	0.6	0.02
M21	6.1	8.9	-	-	0.1	0.08
M22	0.9	-	-	-	-	-
M24	1.5	3.0	3.1	6.6	-	0.06
M26	1.3	-	-	-	-	-
M30	-	6.1	-	-	-	-
M31	-	3.2	-	-	-	-
M34	-	3.4	-	-	-	0.1
M35a	-	MS [h]	-	-	-	-
M35b	-	2.2	-	-	-	-
M36	-	0.9	-	-	-	-
M37a, b [d]	-	1.1	-	-	-	-
Dasatinib	11.2	3.2	41.6	24.7	0.7	0.6

[a] In IV-dosed BDC rats, 67.4% of the radioactive dose was excreted in the bile in 0-12 h interval.

[b] In IV-dosed BDC monkeys, 67% of the radioactive dose was excreted in the bile in 0-72 h interval.

Downloaded from dmd.aspetjournals.org at ASPET Journals on April 10, 2024

DMD Fast Forward. Published on April 17, 2008 as DOI: 10.1124/dmd.107.018234
This article has not been copyedited and formatted. The final version may differ from this version.

[c] In orally-dosed intact rats and monkeys, 76.4 and 76.8% of the radioactive dose was excreted in the feces and 6.4 and 3.0% of the radioactive dose was excreted in urine, respectively, in the 0-168-h interval post-dose.

[d] Metabolites (M3a,b), (M23, M23a,b), and (M37a,b) were pairs of positional isomers that were not well-resolved from each other chromatographically. The values reported represent the combined percentage for the co-eluting isomers.

[e] In rat bile, metabolites M4 and M6 co-eluted.

[f] In rat bile, metabolite M23 was detected. It is not known whether M23 corresponds to M23a or M23b. M8b was not detected in monkey bile.

[g] In monkey bile, metabolites M8b, M23a, and M23b co-eluted.

[h] Metabolite M35a was detected only by mass spectrometry.

Downloaded from dmd.aspetjournals.org at ASPET Journals on April 10, 2024

TABLE 4

Mass-spectral characterization of dasatinib metabolites identified in in vitro incubations with liver microsomes and hepatocytes from rats, monkeys, and humans, and in plasma, urine, bile and feces samples collected after administration of a single oral or IV dose of [^{14}C]dasatinib to rats and monkeys

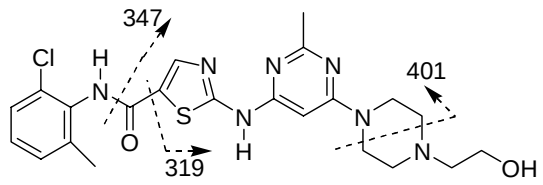

Dasatinib

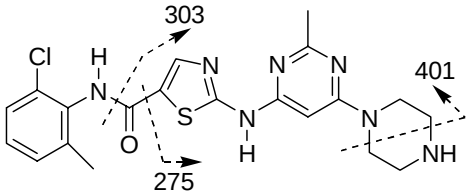

M4

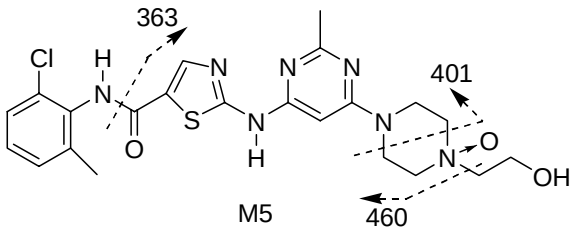

M5

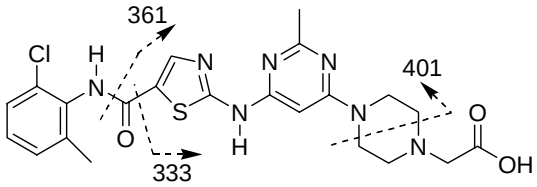

M6

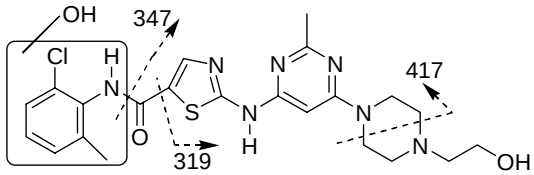

M20 or M24

Metabolite	[M+H]$^+$	Major Fragment Ions	Metabolic Pathway(s)	Species[a]		
P, parent drug	488	401, 347, 319, 260, 232[b]	-	*rat*	*monkey*	*human*
M3a, M3b	520	502, 476, 433, 417, 363	Hydroxylation, *N*-oxidation	*rat*	*monkey*	*human*
M4	444	401, 303, 275, 260, 232	*N*-dealkylation	*rat*	*monkey*	*human*
M5	504	460, 427, 401, 363	*N*-oxidation	*rat*	*monkey*	*human*
M6	502	458, 401, 361, 333	Formation of a carboxylic acid	*rat*	*monkey*	*human*
M7	518	456, 439, 401, 375, 315	Hydroxylation, acid formation	*rat*	*monkey*	*human*
M8, M8a, M8b, M8c[c]	664	488, 401, 347, 319	Glucuronide conjugation	*rat*	*monkey*	-

Downloaded from dmd.aspetjournals.org at ASPET Journals on April 10, 2024

DMD Fast Forward. Published on April 17, 2008 as DOI: 10.1124/dmd.107.018234
This article has not been copyedited and formatted. The final version may differ from this version.

M9	486	399, 347, 319, 263	Dehydrogenation	-	*monkey*	*human*
M13 [c]	568	488, 401, 347, 319	Sulfate conjugation	*rat*	-	-
M14 [c, d]	462	401, 375, 321	*N*-dealkylation, piperazine ring-opening	*rat*	-	-
M15 [c, d]	520	502, 401, 379	Bis-oxygenation	*rat*	-	-
M20	504	417, 347, 319	Hydroxylation	*rat*	*monkey*	*human*
M21	584	504, 417, 347	Hydroxylation, sulfate conjugation	*rat*	*monkey*	*human*
M22 [c, d]	504	486, 401, 375	Hydroxylation	*rat*	-	-
M23, M23a, M23b	518	500, 417, 361, 333	Hydroxylation, acid formation	*rat*	*monkey*	*human*
M24	504	486 (-H_2O), 417, 399, 347	Hydroxylation	*rat*	*monkey*	*human*
M26 [c, d]	609	468, 456, 444, 401	Taurine conjugation	*rat*	-	-
M28a, M28b [e]	460	442, 417, 303, 275	Hydroxylation, *N*-dealkylation	-	*monkey*	*human*
M29a, M29b, M29c [e]	520	502, 433, 397, 347	Bis-hydroxylation	-	*monkey*	*human*
M30	598	518, 417, 361, 333	Hydroxylation, N-dealkylation, sulfate conjugation	-	*monkey*	*human*
M31	600	520, 433, 397, 347	Bis-hydroxylation, sulfate conjugation	-	*monkey*	-
M34 [c]	534	472, 403, 377, 333	Hydroxylation, *N*-oxidation, acid formation	-	*monkey*	-
M35a, M35b [c]	662	486, 399, 347, 319	Dehydrogenation, glucuronide conjugation	-	*monkey*	-
M36 [c]	694	518, 417, 361, 333	Hydroxylation, acid formation, glucuronide conjugation	-	*monkey*	-
M37a, M37b [c]	680	504, 486, 417, 347	Hydroxylation, glucuronide conjugation	-	*monkey*	

[a] For rat and monkey, metabolites were identified from both in vitro incubations and in vivo samples. Human metabolites were identified in *in vitro* liver microsomal and hepatocyte incubations only.
[b] Accurate mass analysis of the major fragment ions of dasatinib indicated that the observed masses were all within 4 ppm of their theoretical values.
[c] These metabolites were found in *in vivo* samples but were not formed in vitro.
[d] These metabolites were identified in BDC rats, but not intact rats.
[e] These metabolites were formed in samples from in vitro incubations but were not found in *in vivo* samples.

Downloaded from dmd.aspetjournals.org at ASPET Journals on April 10, 2024

DMD Fast Forward. Published on April 17, 2008 as DOI: 10.1124/dmd.107.018234
This article has not been copyedited and formatted. The final version may differ from this version.

DMD Fast Forward. Published on April 17, 2008 as DOI: 10.1124/dmd.107.018234
This article has not been copyedited and formatted. The final version may differ from this version.

TABLE 5

Key NMR data for metabolites M20 (4-OH, M24 (7-OH) and dasatinib

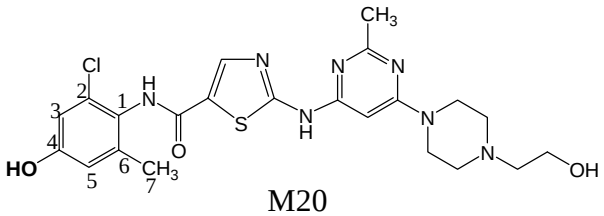

M20

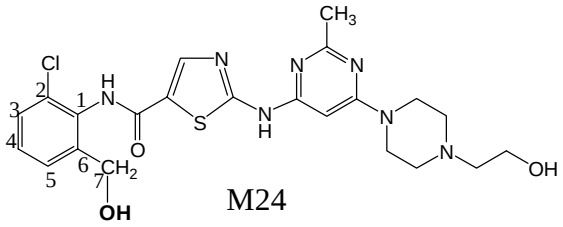

M24

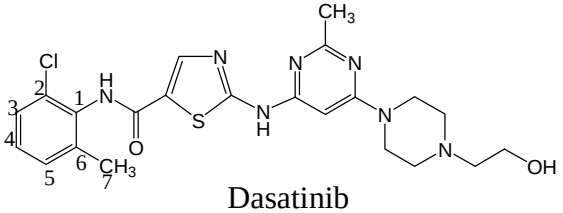

Dasatinib

Position	**M20** (4-OH)			**M24** (7-OH)	**Dasatinib**
	^{1}H ppm (mult, *J* =Hz)	^{13}C ppm	HMBC (^{1}H-^{13}C correlation)	^{1}H ppm (mult, *J* =Hz)	^{1}H ppm (mult, *J* =Hz)
1	n/a	125	n/a	n/a	n/a
2	n/a	133	n/a	n/a	n/a
3	6.77 (d, *J*=2.65)	113.8	C1, C2, C4, C5	7.56 (d, *J*=8.0)	7.41 (d, *J*=7.5)
4	n/a	157	n/a	7.46 (t, *J*=8.0)	7.27 (t, *J*=7.5)
5	6.67 (d, *J*=2.65)	116.3	C1, C3, C4	7.53 (d, *J*=8.0)	7.30 (d, *J*=7.5)
6	n/a	139	n/a	n/a	n/a
7	2.14 (s)	18.8	C1, C5, C6	4.54 (s)	2.25 (s)

n/a: not applicable

Downloaded from dmd.aspetjournals.org at ASPET Journals on April 10, 2024

Figure 1

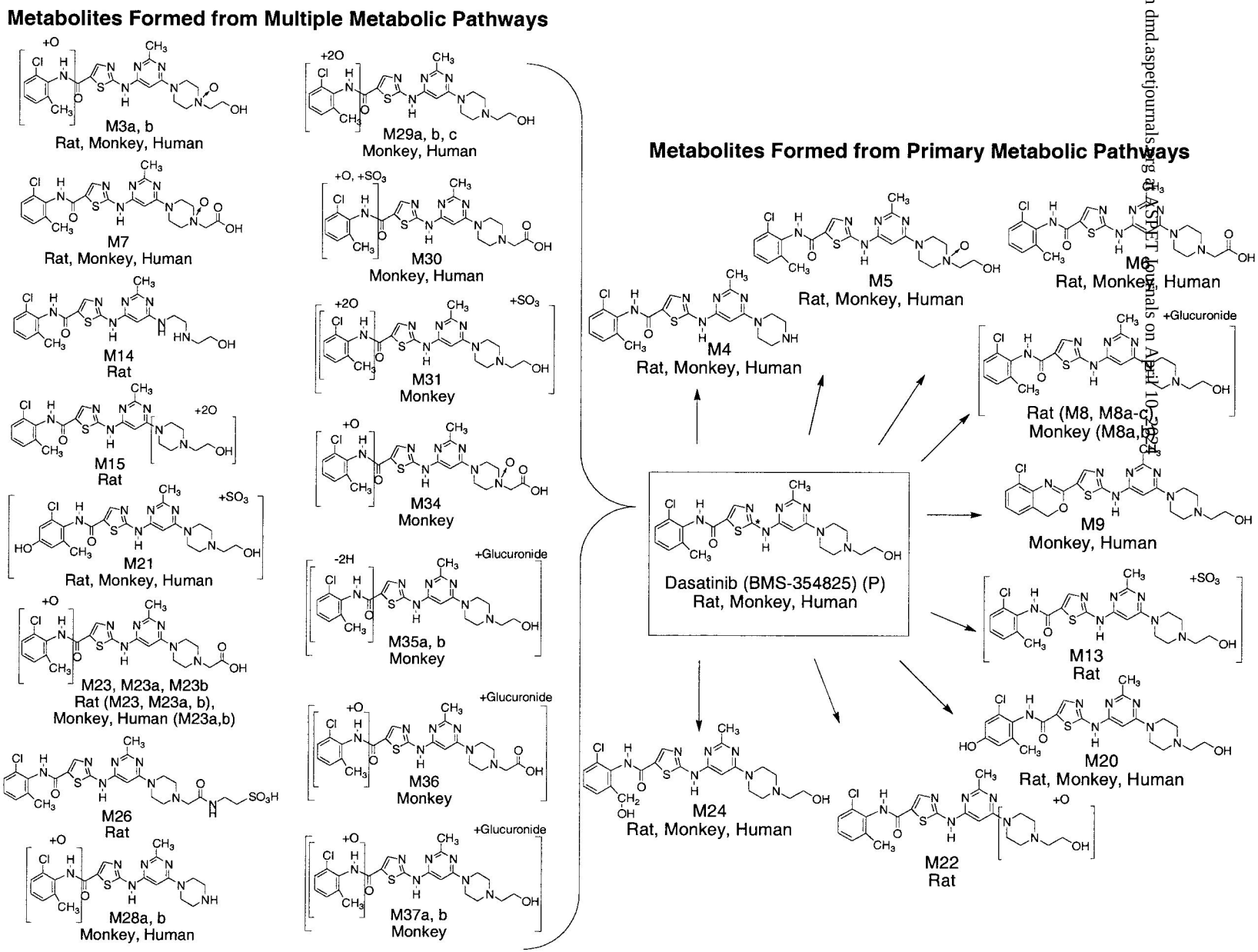

Downloaded from dmd.aspetjournals.org at ASPET Journals on April 10, 2024

Figure 2

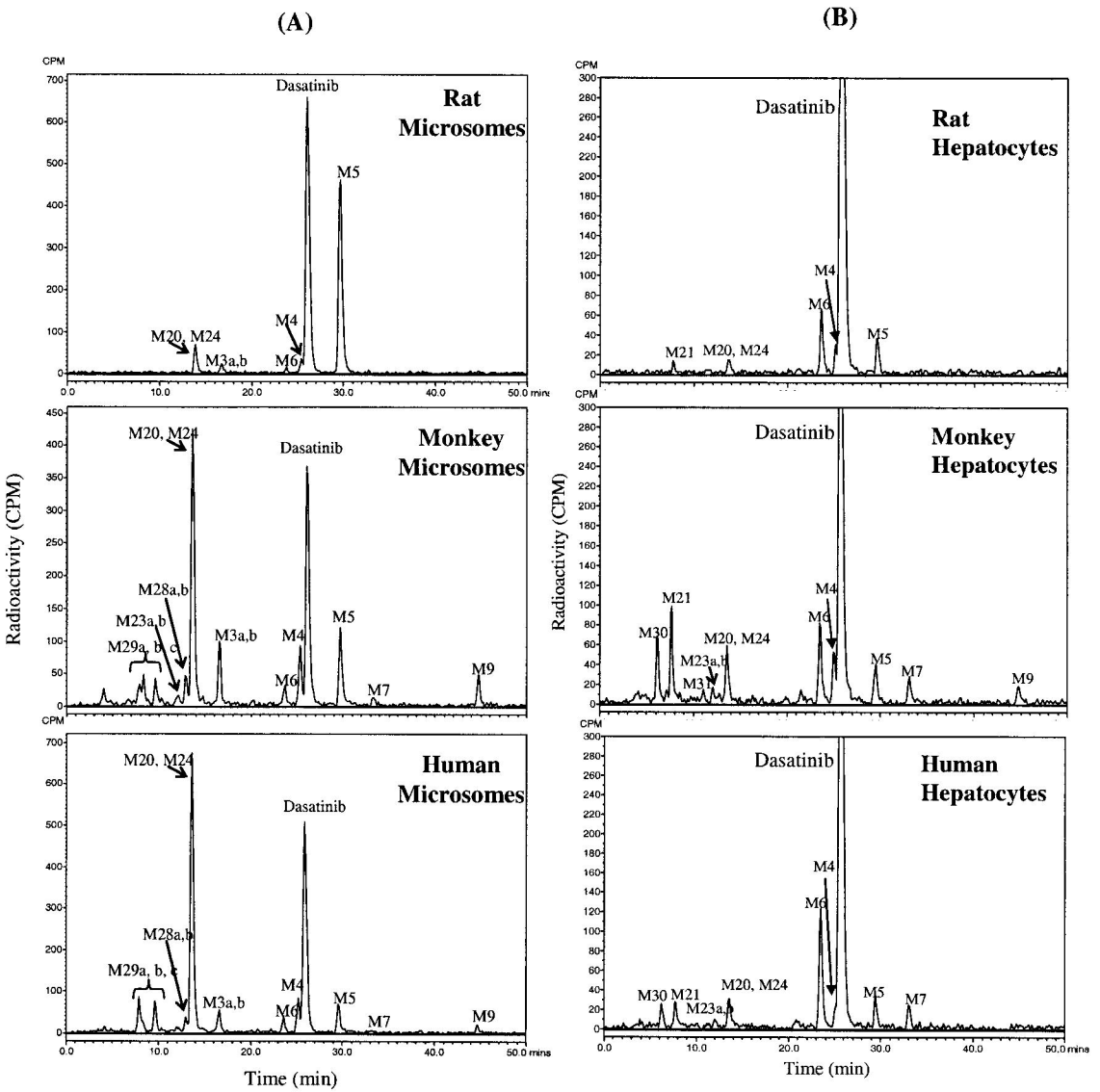
(A)
(B)
Rat Microsomes
Monkey Microsomes
Human Microsomes
Rat Hepatocytes
Monkey Hepatocytes
Human Hepatocytes
Dasatinib
M20, M24
M3a,b
M4
M6
M5
M7
M9
M21
M30
M23a,b
M28a,b
M29a, b, c
CPM
Radioactivity (CPM)
Time (min)

Figure 3

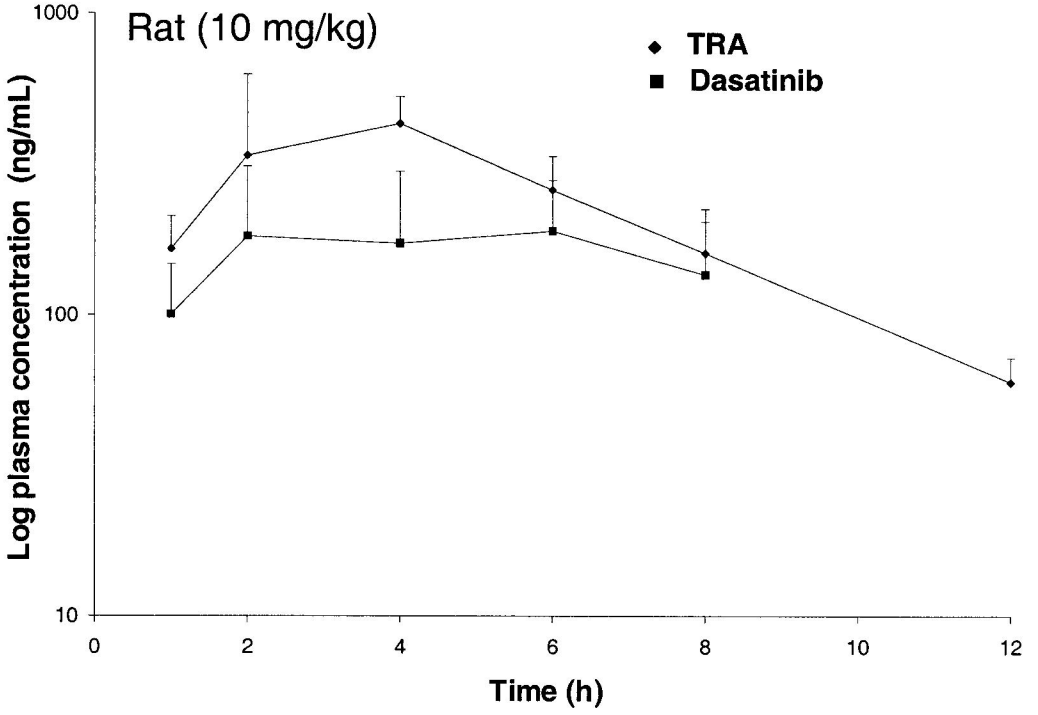
Rat (10 mg/kg)
TRA
Dasatinib
Log plasma concentration (ng/mL)
1000
100
10
0
2
4
6
8
10
12
Time (h)

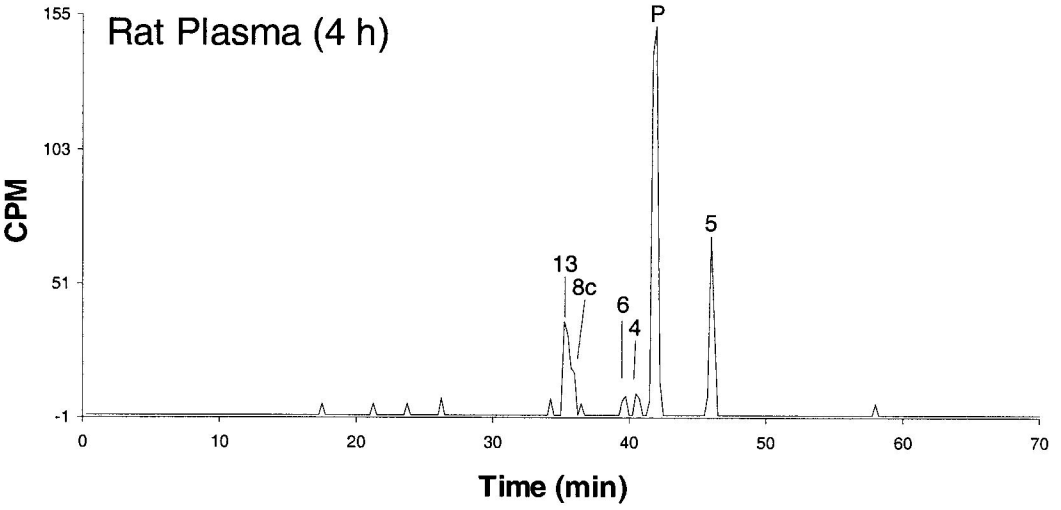
Rat Plasma (4 h)
CPM
155
103
51
-1
P
5
13
8c
6
4
0
10
20
30
40
50
60
70
Time (min)

Figure 4

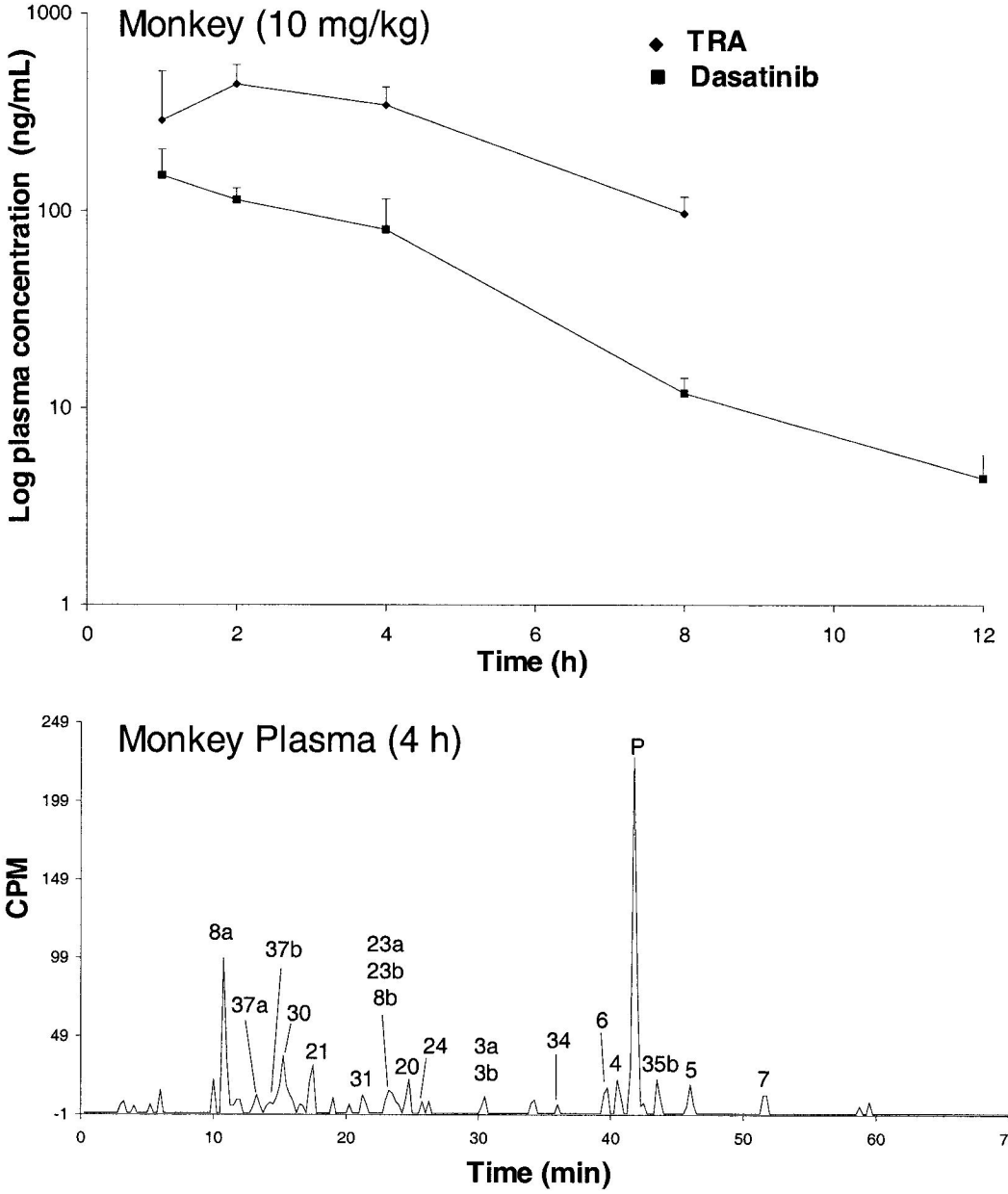
Monkey (10 mg/kg)
TRA
Dasatinib
Log plasma concentration (ng/mL)
1000
100
10
1
0
2
4
6
8
10
12
Time (h)
Monkey Plasma (4 h)
CPM
249
199
149
99
49
-1
8a
37b
37a
30
21
31
23a
23b
8b
20
24
3a
3b
34
6
4
P
35b
5
7
0
10
20
30
40
50
60
70
Time (min)

Figure 5

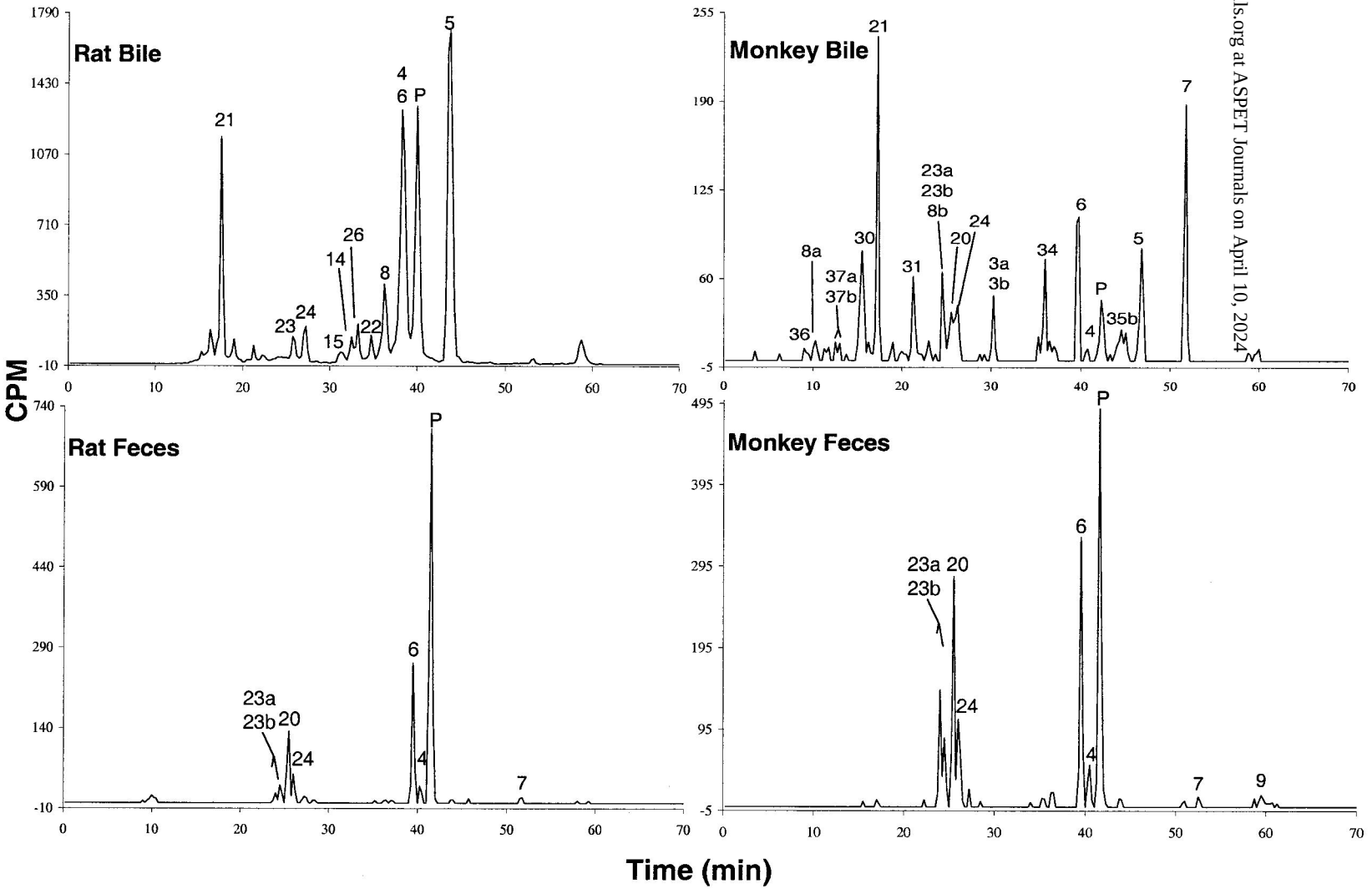

d from dmd.aspetjournals.org at ASPET Journals on April 10, 2024

Figure 6

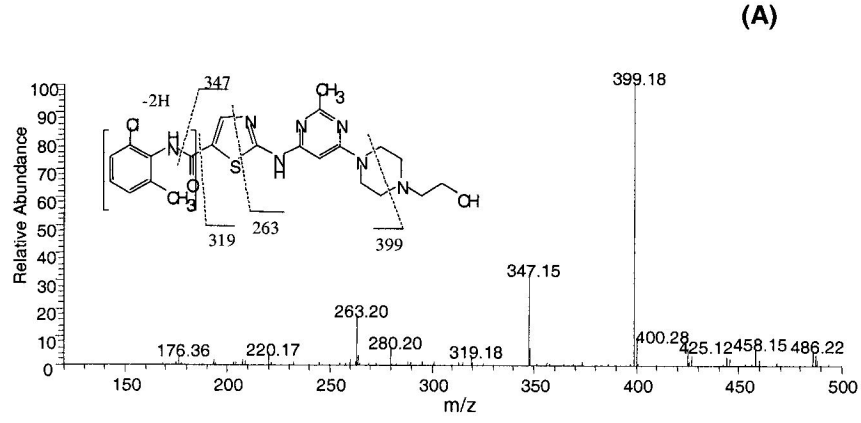
(A)
-2H
347
319
263
399
399.18
347.15
263.20
280.20
319.18
176.36
220.17
400.28
425.12
458.15
486.22
Relative Abundance
m/z

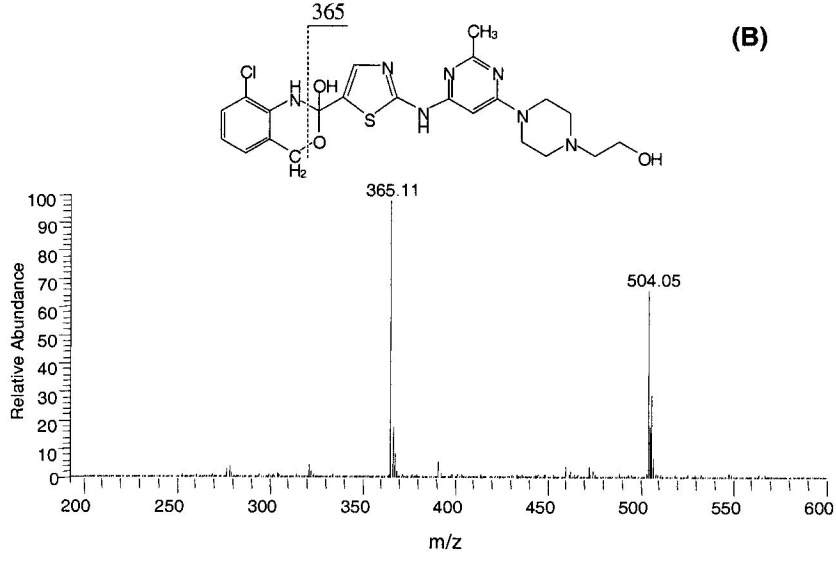
(B)
365
365.11
504.05
Relative Abundance
m/z

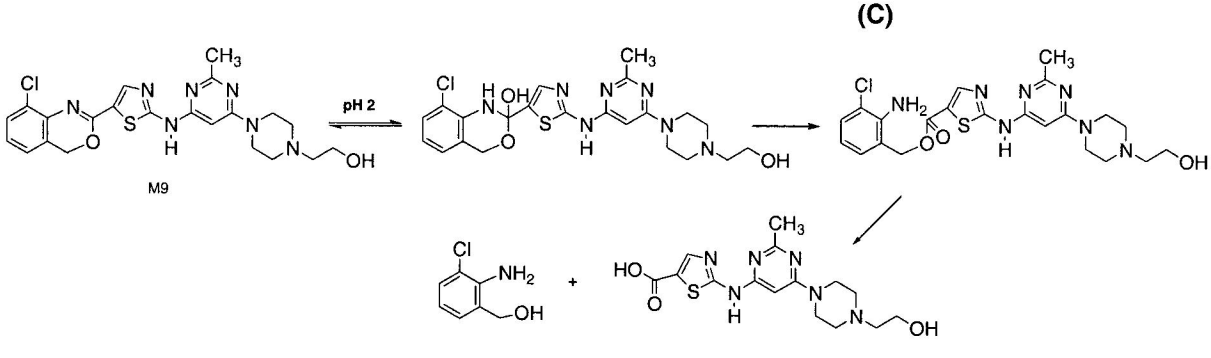
(C)
pH 2
M9

Figure 7

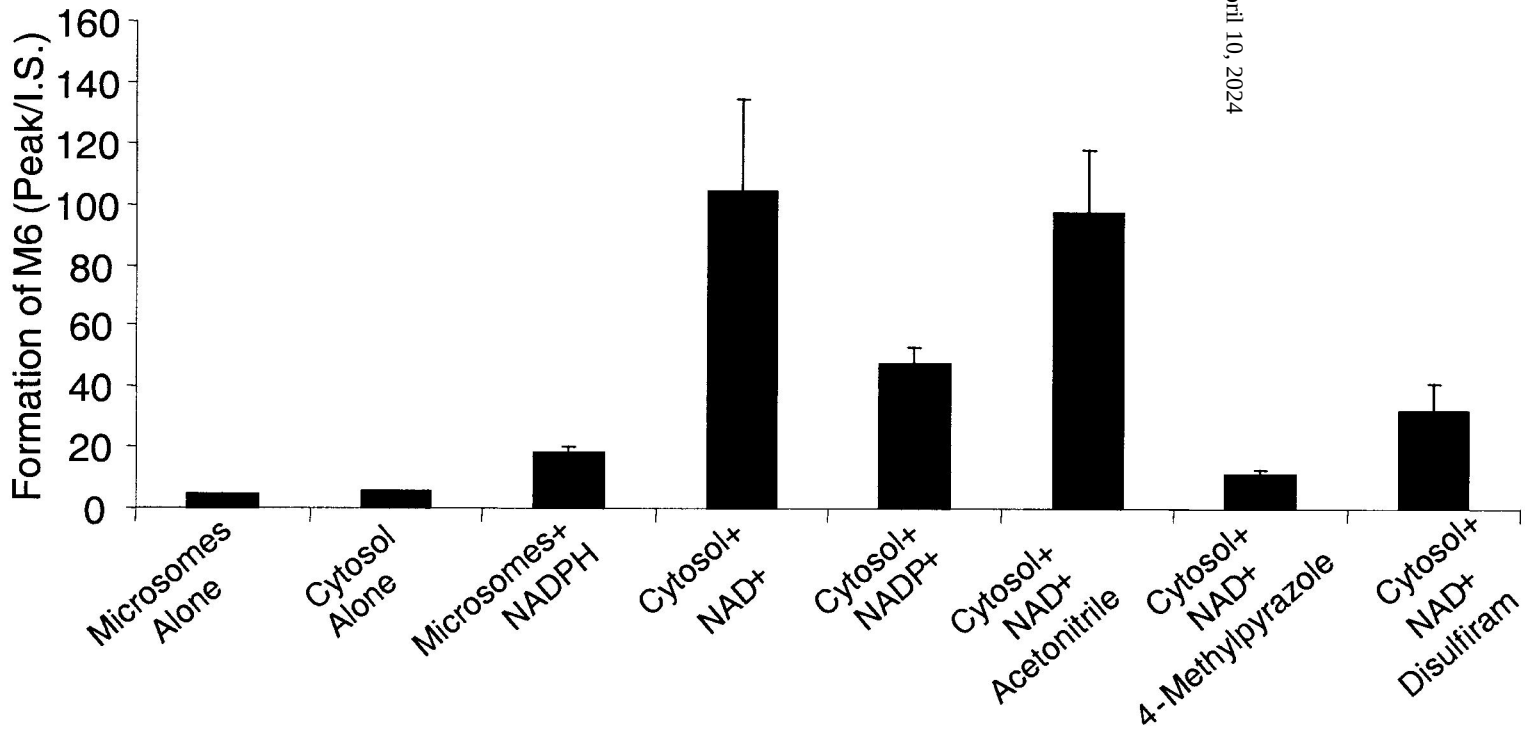

ded from dmd.aspetjournals.org at ASPET Journals on April 10, 2024